Journal of Inorganic Biochemistry 202 (2020) 110857

Contents lists available at ScienceDirect

Journal of Inorganic Biochemistry

journal homepage: www.elsevier.com/locate/jinorgbio

Synthesis, characterization, DNA/BSA interactions and in vitro cytotoxicity study of palladium(II) complexes of hispolon derivatives

Xiaonan Wei[a,b,1], Yaxing Yang[a,b,1], Jiangfeng Ge[a,b], Xue Lin[a,b], Dandan Liu[a,b,*], Shuxiang Wang[a,b], Jinchao Zhang[a,b], Guoqiang Zhou[a,b,*], Shenghui Li[a,b,*]

[a] Key Laboratory of Medicinal Chemistry and Molecular Diagnosis of Ministry of Education, Hebei University, Baoding 071002, China
[b] Key Laboratory of Chemical Biology of Hebei Province, College of Chemistry & Environmental Science, Hebei University, Baoding 071002, China

ARTICLE INFO

Keywords:
Palladium(II) complexes
Hispolon
Reactive oxygen species (ROS)
Apoptosis
Antitumor

ABSTRACT

Thirteen novel palladium(II) complexes of the general formula [Pd(bipy)(*O*,*O*′-dkt)](PF_6), (where bipy is 2,2′-bipyridine and *O*,*O*′-dkt is β-diketonate ligand hispolon or its derivative) have been prepared through a metal-ligand coordination method that involves spontaneous formation of the corresponding diketonate scaffold. The obtained palladium(II) complexes have been characterized by NMR spectroscopy, ESI-mass spectrometry as well as elemental analysis. The cytotoxicity analysis indicates that most of the obtained palladium(II) complexes show promising growth inhibition in three human cancer cell lines. Flow cytometry analysis shows complex **3e** could promote intracellular reactive oxygen species (ROS) accumulation and lead cancer cell death. And the suppression of ROS accumulation and the rescue of cell viability in HeLa cells by *N*-acetyl-L-cysteine (NAC) suggest the possible link between the increase in ROS generation and cytotoxicity of complex **3e**. Flow cytometry analysis also reveal that complex **3e** cause cell cycle arrest in the G2/M phase and collapse of the mitochondrial membrane potential, promote the generation of ROS and lead to tumor cell apoptosis. The interactions of complex **3e** with calf thymus DNA (CT-DNA) have been evaluated by UV–Vis spectroscopy, fluorescence quenching experiments and viscosity measurements, which reveal that the complex interact with CT-DNA through minor groove binding and/or electrostatic interactions. Further, the results of fluorescence titration and site marker competitive experiment on bovine serum albumin (BSA) suggest that complex **3e** can quench the fluorescence of BSA via a static quenching process and bind to BSA in Sudlow's site II.

1. Introduction

Platinum-based antineoplastic drugs (cisplatin, carboplatin, and oxaliplatin) have long played an important role in the clinical treatment of human malign tumor [1]. However, severe toxic side effects and intrinsic or acquired drug resistance limit their applicability and chemotherapeutic efficacy [2]. In addition to nonclassical platinum(II) complexes [3], considerable attempts are also being made to replace these classical platinum drugs with suitable alternatives, and numerous transition metal complexes other than platinum have been synthesized and screened for their antitumor activities in the past decades [4].

In addition to excellent catalytic performance, palladium(II) complexes have recently been studied as potential chemotherapeutic agents against cancer, partly due to its structural and thermodynamic similarities with platinum(II) complexes [5,6]. Investigations have shown that some Pd (II) complexes exhibit similar or even better anti-tumor activity than cisplatin and its analogues [7–12]. Unfortunately, the potential therapeutic application of Pd (II) complexes is severely complicated by its lower in vivo stability and multiple speciation due to their higher reactivities toward biomolecules [13,14]. Mixed ligand complexes are characterized by their extreme stability. Therefore, it is natural that there are studies in which strongly coordinated chelate nitrogen ligands and an appropriate O,O′- bidentate chelating ligands as leaving group has been exploited to improve the stability of palladium (II) antitumor complexes [15].

N,*N*-chelating ligand, including bipyridine, quinoline, phenanthroline and their derivatives, were widely utilized as bidentate ligands in the field of antitumor transition metal chemistry because of their ability to participate as DNA intercalators [16,17]. Among which, 2,2′-bipyridyls are favoured ligand scaffolds that have drawn special attention due to their presence in natural product molecules such as caerulomycins or collismycins [18–20]. The properties of β-diketones are of

* Corresponding authors at: Key Laboratory of Medicinal Chemistry and Molecular Diagnosis of Ministry of Education, Hebei University, Baoding 071002, China.
E-mail addresses: leo-liudan@163.com (D. Liu), zhougq1982@163.com (G. Zhou), lish@hbu.edu.cn (S. Li).
[1] These authors contributed equally to this work.

https://doi.org/10.1016/j.jinorgbio.2019.110857
Received 27 February 2019; Received in revised form 17 August 2019; Accepted 12 September 2019
Available online 05 October 2019
0162-0134/

interest due to their application as metal extracting agents and key intermediates to various heterocyclic compounds. Furthermore, some β-diketones also exhibit anecdotal extent of biogical activities, such as antibacterial, antiviral, insecticidal, antioxidant, as well as potential antitumor activities [21]. Although the corresponding β-diketonates of this class of compounds have been utilized as functional or structural scaffolds for titanium(IV) [22,23], platinum(II) [24–28], copper(II) [29–31], rhodium(I) [32], iridium(I) [33], lanthanide(III) [34,35], molybdenum(VI), cobalt(II) [36] and organometallic ruthenium(II) anticancer agents [37–41], few studies describe their potential utility in palladium-based therapeutic agents. Recently, Valentini and co-workers have prepared a palladium(II) complex incorporating deprotonated curcumin. The complexation of this biologically active β-diketonate ligand with palladium(II) led to the formion of a more stable species and improved the bioavailability of curcumin to some extent. However, the reported complex showed lower cytotoxicity than pure curcumin alone [42]. Very recently, our group has founded that the cytotoxicity of curcuminoid palladium complex was closely realted to the aryl substituents [43], similar to the reported structure–activity relationships (SAR) of arene-ruthenium(II) curcuminoid complexes [44].

Hispolon, isolated initially from *Inonotus Hispidus* [45] , is a polyphenolic compound with β-diketone functional group. As a structural analogue of curcumin, hisponlon has also been reported to show numerous pharmacological properties such as antiviral [46], hepatoprotective [47], immunomodulatory [48], anti-inflammatory [49], antiproliferative activities [50–52] in different models. Among which, the anticancer activity of hispolon was found to work through a variety of mechanisms such as induction of G0/G1cell cycle arrest and cell apoptosis, enhancement of p53-dependent gene activation and suppression of tumor metastasis [50–54]. Importantly, some of the studies have demonstrated that hispolon is non-toxic to most normal cells. However, the pharmacological application of hispolon, in some degree, is hampered by its chemical instability under physiological conditions [55]. It is generally accepted that the physiological instability of hispolon, partly owing to the existence of the β-diketone moiety or the conjugated diene structure in its two possible tautomers structure, attributes its low bioavailability, just as that of curcumin. The chemical structures of curcumin, hispolon and one typical example of its derivatives studied in the present research are shown in Scheme 1.

With the aim to mitigate the inherent disadvantage of hispolon and broaden its potential applications in anticancer metallodrug strategy, a family of cationic Pd(II) complex of hispolon or its derivatives have been prepared through a metal-ligand coordination method which includes spontaneous formation of the corresponding diketonate scaffold in aqueous acetone solution. To elucidate the structure-activity relationships (SAR) and cytotoxic mechanisms of these complexes, DNA/human serum albumin (BSA) interactions, antiproliferative effect, prooxidative effect, reactive oxygen species (ROS)-mediated apoptosis, cell cycle arrest, and the associated mitochondrial dysfunction were investigated.

2. Experimental section

2.1. Materials and methods

All reagents and chemicals purchased were of reagent grade and used without further purification. Dulbecco's modified eagle's medium (DMEM), trypsin and fetal bovine serum (FBS) were purchased from Gibco (Grand Island, NY, USA). 3-(4,5-dimethylthiazol-2-yl)-2,5-diphenyl tetrazolium bromide (MTT), 2′,7′-dichlorodihydrofluoroscein diacetate (DCFH-DA), benzylpenicillin, streptomycin and calf-thymus DNA (CT-DNA) were purchased from Sigma-Aldrich (St. Louis, MO, USA). Annexin V-fluorescein isothiocyanate (FITC)/propidium iodide (PI) apoptosis detection kit was purchased from BestBio (Shanghai China). Mitochondrial membrane potential assay kit with 5,5′,6,6′-tetrachloro-1,1′,3,3′-tetraethylbenzimidazolcarbocyanine iodide (JC-1) was purchased from Beyotime (China). ^{1}H and ^{13}C NMR spectra were obtained on a Bruker AVIII 600 spectrometer. The chemical shifts (δ) of proton and carbon are reported with tetramethylsilane (TMS) as an internal standard. The mass spectra were measured by LC-MS apparatus Agilent 1200-6310. Elemental analysis (C, H and N) was performed on an Elementar Vario EL III elemental analyzer. Melting points were measured on a XT-4 microscopic melting-point spectrometer without correlation.

2.2. Synthesis of complexes

2.2.1. Preparation of ligand related to hispolon **2a-2m**

General procedure: 2,4-pentanedione (2.0 g, 20 mmol), boron oxide (2.0 g, 28 mmol) and tributyl borate solution (3 mL) were added to an oven-dried three-neck flask, the resulted mixture was stirred for 0.5 h at 90 °C. Followed by the addition of different substituted benzaldehyde (4 mmol), the mixture of n-butyl amine (0.5 mL) and tributyl borate (2 mL) were added dropwise during 30 min and the obtained mixture was further stirred for 4 h at 85 °C. Then reaction mixture was gradually cooled to 50 °C and acidified by 0.4 M HCl (to pH = 4), and extracted three times with ethyl acetate (3 × 100 mL). The organic phase was washed with distilled water, dried over anhydrous Na_2SO_4, filtrated, and concentrated under vacuum. The residue was purified by column chromatography using petroleum ether and ethyl acetate (20:1) as eluants to obtain a yellow solid.

*2.2.1.1. (3Z,5E)-4-hydroxy-6-(2-methoxyphenyl)hexa-3,5-dien-2-one **(2a)***. Yellow solid, Yield: 56%. ^{1}H NMR (600 MHz, $CDCl_3$) δ: 15.46 (s, 1H, enol-OH), 7.91 (d, J = 15.6 Hz, 1H, H6), 7.48 (d, J = 7.8 Hz, 1H, Ar—H6), 7.30 (t, J = 7.8 Hz, 1H, Ar—H4), 6.93 (t, J = 7.8 Hz, 1H, Ar—H5), 6.87 (d, J = 7.8 Hz, 1H, Ar—H3), 6.54 (d, J = 15.6 Hz, 1H, H5), 5.63 (s, 1H, H3), 3.84 (s, 3H, OCH_3-2), 2.13 (s, 3H, CH_3).

*2.2.1.2. (3Z,5E)-4-hydroxy-6-(3-methoxyphenyl)hexa-3,5-dien-2-one **(2b)***. Yellow solid, Yield: 45%. ^{1}H NMR (600 MHz, DMSO-d_6) δ: 7.53 (d, J = 15.6 Hz, 1H, H6), 7.33 (t, J = 7.8 Hz, 1H, Ar—H5), 7.26 (br s, 1H, Ar—H2), 7.25 (d, J = 9.6 Hz, 1H, Ar—H6), 6.97 (dd, J_1 = 7.8 Hz, J_2 = 1.2 Hz, 1H, Ar—H4), 6.83 (d, J = 15.6 Hz, 1H, H5), 5.91 (s, 1H, H3), 3.80 (s, 3H, OCH_3-3), 2.15 (s, 3H, CH_3).

*2.2.1.3. (3Z,5E)-4-hydroxy-6-(4-methoxyphenyl)hexa-3,5-dien-2-one **(2c)***. Yellow solid, Yield: 50%. ^{1}H NMR (600 MHz, $CDCl_3$) δ: 15.48 (s, 1H, enol-OH), 7.56 (d, J = 15.6 Hz, 1H, H6), 7.47 (d, J = 9.0 Hz, 2H, Ar—H2 and Ar—H6), 6.91 (d, J = 9.0 Hz, 2H, Ar—H3 and Ar—H5), 6.34 (d, J = 15.6 Hz, 1H, H5), 5.62 (s, 1H, H3), 3.84 (s, 3H, OCH_3–4), 2.15 (s, 3H, CH_3).

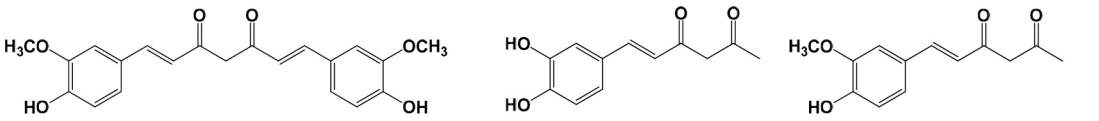

Curcumin Hispolon Monophenyl curcumin (half-curcumin)

Scheme 1. Chemical structures of curcumin, hispolon and one of its derivative.

*2.2.1.4. (3Z,5E)-6-(3,4-dimethoxyphenyl)-4-hydroxyhexa-3,5-dien-2-one **(2d)***. Yellow solid, Yield: 48%. ^{1}H NMR (600 MHz, $CDCl_3$) δ: 15.48 (br s, 1H, enol-OH), 7.55 (d, J = 15.6 Hz, 1H, H6), 7.11 (dd, J_1 = 8.4 Hz, J_2 = 1.8 Hz, 1H, Ar—H6), 7.06 (d, J = 1.8 Hz, 1H, Ar—H2), 6.87 (d, J = 8.4 Hz, 1H, Ar—H5), 6.35 (d, J = 15.6 Hz, 1H, H5), 5.64 (s, 1H, H3), 3.93 (s, 3H, OCH_3-3), 3.92 (s, 3H, OCH_3-4), 2.16 (s, 3H, CH_3).

*2.2.1.5. (3Z,5E)-6-(3,5-dimethoxyphenyl)-4-hydroxyhexa-3,5-dien-2-one **(2e)***. Yellow solid, Yield: 46%. ^{1}H NMR (600 MHz, $CDCl_3$) δ: 15.30 (s, 1H, enol-OH), 7.51 (d, J = 15.6 Hz, 1H, H6), 6.66 (d, J = 1.8 Hz, 2H, Ar—H2 and Ar—H6), 6.48 (s, 1H, Ar—H4), 6.43 (d, J = 15.6 Hz, 1H, H5), 5.66 (s, 1H, H3), 3.82 (s, 6H, OCH_3-3 and OCH_3-5), 2.18 (s, 3H, CH_3).

*2.2.1.6. (3Z,5E)-4-hydroxy-6-(3,4,5-trimethoxyphenyl)hexa-3,5-dien-2-one **(2f)***. Yellow solid, Yield: 49%. ^{1}H NMR (600 MHz, $CDCl_3$) δ: 15.38 (s, 1H, enol-OH), 7.51 (d, J = 15.6 Hz, 1H, H6), 6.75 (s, 2H, Ar—H2 and Ar—H6), 6.37 (d, J = 15.6 Hz, 1H, H5), 5.66 (s, 1H, H3), 3.90 (s, 6H, OCH_3-3 and OCH_3-5), 3.89 (s, 3H, OCH_3-4), 2.17 (s, 3H, CH_3).

*2.2.1.7. (3Z,5E)-4-hydroxy-6-(3-hydroxyphenyl)hexa-3,5-dien-2-one **(2g)***. Yellow solid, Yield: 30%. ^{1}H NMR (600 MHz, $CDCl_3$) δ: 15.28 (s, 1H, enol-OH), 7.53 (d, J = 15.6 Hz, 1H, H6), 7.25 (t, J = 7.8 Hz, 1H, Ar—H5), 7.09 (d, J = 7.8 Hz, 1H, Ar—H6), 6.99 (s, 1H, Ar—H2), 6.85 (dd, J_1 = 7.8 Hz, J_2 = 1.8 Hz, 1H, Ar—H4), 6.43 (d, J = 15.6 Hz, 1H, H5), 5.65 (s, 1H, H3), 2.18 (s, 3H, CH_3).

*2.2.1.8. (3Z,5E)-4-hydroxy-6-(4-hydroxyphenyl)hexa-3,5-dien-2-one **(2h)***. Yellow solid, Yield: 49%. ^{1}H NMR (600 MHz, $CDCl_3$) δ: 15.41 (s, 1H, enol-OH), 7.50 (d, J = 15.6 Hz, 1H, H6), 7.43 (d, J = 8.4 Hz, 2H, Ar—H2 and Ar—H6), 6.85 (d, J = 8.4 Hz, 2H, Ar—H3 and Ar—H5), 6.34 (d, J = 15.6 Hz, 1H, H5), 5.63 (s, 1H, H3), 2.16 (s, 3H, CH_3).

*2.2.1.9. (3Z,5E)-6-(3,4-dihydroxyphenyl)-4-hydroxyhexa-3,5-dien-2-one **(2i, hispolon)***. Yellow solid, Yield: 38%. ^{1}H NMR (600 MHz, $CDCl_3$) δ: 7.48 (d, J = 15.6 Hz, 1H, H6), 7.07 (d, J = 1.8 Hz, 1H, Ar—H2), 7.01 (dd, J_1 = 7.8 Hz, J_2 = 1.8 Hz, 1H, Ar—H6), 6.87 (d, J = 7.8 Hz, 1H, Ar—H5), 6.29 (d, J = 15.6 Hz, 1H, H5), 5.62 (s, 1H, H3), 2.16 (s, 3H, CH_3).

*2.2.1.10. (3Z,5E)-6-(3,5-dihydroxyphenyl)-4-hydroxyhexa-3,5-dien-2-one **(2j)***. Yellow solid, Yield: 57%. ^{1}H NMR (600 MHz, DMSO-d_6) δ: 15.50 (s, 1H, enol-OH), 7.35 (d, J = 16.2 Hz, 1H, H6), 6.59 (d, J = 16.2 Hz, 1H, H5), 6.49 (d, J = 1.2 Hz, 2H, Ar—H2 and Ar—H6), 6.29 (s, 1H, Ar—H4), 5.93 (s, 1H, H3), 2.14 (s, 3H, CH_3).

*2.2.1.11. (3Z,5E)-4-hydroxy-6-(4-hydroxy-3-methoxyphenyl)hexa-3,5-dien-2-one **(2k)***. Yellow solid, Yield: 39%. ^{1}H NMR (600 MHz, $CDCl_3$) δ: 15.49 (br s, 1H, enol-OH), 7.53 (d, J = 16.2 Hz, 1H, H6), 7.10 (br s, 1H, Ar—H5), 7.02 (s, 1H, Ar—H2), 6.92 (br s, 1H, Ar—H6), 6.32 (d, J = 16.2 Hz, 1H, H5), 5.94 (s, 1H, Ar-OH), 5.63 (s, 1H, H3), 3.93 (s, 3H, OCH_3-3), 2.16 (s, 3H, CH_3).

*2.2.1.12. (3Z,5E)-4-hydroxy-6-(3-hydroxy-4-methoxyphenyl)hexa-3,5-dien-2-one **(2l)***. Yellow solid, Yield: 52%. ^{1}H NMR (600 MHz, $CDCl_3$) δ: 15.44 (s, 1H, enol-OH), 7.51 (d, J = 15.6 Hz, 1H, H6), 7.14 (s, 1H, Ar—H2), 7.02 (d, J = 7.8 Hz, 1H, Ar—H6), 6.84 (d, J = 7.8 Hz, 1H, Ar—H5), 6.32 (d, J = 15.6 Hz, 1H, H5), 5.69 (br s, 1H, Ar-OH), 5.62 (s, 1H, H3), 3.93 (s, 3H, OCH_3-4), 2.16 (s, 3H, CH_3).

*2.2.1.13. (3Z,5E)-6-(benzo[d][1,3]dioxol-5-yl)-4-hydroxyhexa-3,5-dien-2-one **(2m)***. Yellow solid, Yield: 54%. ^{1}H NMR (600 MHz, $CDCl_3$) δ: 15.43 (s, 1H, enol-OH), 7.51 (d, J = 16.2 Hz, 1H, H6), 7.03 (d, J = 1.8 Hz, 1H, Ar—H2), 7.00 (dd, J_1 = 7.8 Hz, J_2 = 1.8 Hz, 1H, Ar—H6), 6.81 (d, J = 8.4 Hz, 1H, Ar—H5), 6.29 (d, J = 16.2 Hz, 1H, H5), 6.00 (s, 2H, methylene), 5.61 (s, 1H, H3), 2.15 (s, 3H, CH_3).

*2.2.2. Synthesis of the complexes **3a-3m***

The mixture of hispolon analogs **2a-2m** (0.26 mmol) and (bipy)Pd$(ONO_2)_2$ (0.26 mmol) (where bipy = 2,2′-bipyridine) was stirred in 10 mL of aqueous acetone solution (1:1, *V*/V) at 60 °C for 10 h. The cationic palladium(II) complex **3** (**3a-3m**) as hexaflourophosphate salts were achieved by subsequent anion exchange with KPF_6.

*2.2.2.1. Complex **3a***. Yellow solid, Yield: 94%. ^{1}H NMR (600 MHz, DMSO-d_6) δ: 8.57 (d, J = 7.8 Hz, 1H, Bipy-H6), 8.55 (d, J = 7.8 Hz, 1H, Bipy-H6′), 8.49 (d, J = 5.4 Hz, 1H, Bipy-H3), 8.44 (d, J = 5.4 Hz, 1H, Bipy-H3′), 8.41 (t, J = 7.8 Hz, 1H, Bipy-H4), 8.37 (t, J = 7.8 Hz, 1H, Bipy-H4′), 7.92 (t, J = 6.6 Hz, 1H, Bipy-H5), 7.83 (t, J = 6.6 Hz, 1H, Bipy-H5′), 7.80 (d, J = 15.6 Hz, 1H, H6), 7.67 (d, J = 7.2 Hz, 1H, Ar—H6), 7.44 (t, J = 7.8 Hz, 1H, Ar—H4), 7.10 (d, J = 7.8 Hz, 1H, Ar—H3), 7.01 (t, J = 7.2 Hz, 1H, Ar—H5), 6.88 (d, J = 15.6 Hz, 1H, H5), 5.86 (s, 1H, H3), 3.91 (s, 3H, OCH_3-2), 2.24 (s, 3H, CH_3). ^{13}C NMR (DMSO-d_6, 150 MHz) δ: 188.36(C-2), 177.12(C-4), 157.91(Ar—C2), 155.51(Bipy-C2), 155.22(Bipy-C2′), 146.60(Bipy-C6), 145.93(Bipy-C6′), 142.09(Bipy-C4), 141.93(Bipy-C4′), 136.09(Ar—C1), 131.98(C-6), 128.67(Ar—C4), 127.56(Bipy-C5), 127.53(Bipy-C5′), 124.13(Bipy-C3), 123.99(Bipy-C3′), 123.68(Ar—C6), 122.62(Ar—C5), 120.65(C-5), 111.72(Ar—C3), 103.76(C-3), 55.67(OCH_3-2), 25.89(C-1). ESI-MS (*m/z*): $[M\text{-}PF_6]^+$ calcd for $C_{23}H_{21}N_2O_3Pd$, 479.0; Found: 479.0. Anal. calcd for $C_{23}H_{21}F_6N_2O_3PPd$: C, 44.21; H, 3.39; N, 4.48. Found: C, 43.89; H, 3.43; N, 4.50%.

*2.2.2.2. Complex **3b***. Yellow solid, Yield: 87%. ^{1}H NMR (600 MHz, DMSO-d_6) δ: 8.53 (d, J = 5.4 Hz, 1H, Bipy-H6), 8.51 (d, J = 7.2 Hz, 1H, Bipy-H6′), 8.50 (d, J = 6.6 Hz, 1H, Bipy-H3), 8.40 (d, J = 6.0 Hz, 1H, Bipy-H3′), 8.37 (t, J = 7.8 Hz, 1H, Bipy-H4), 8.34 (t, J = 7.8 Hz, 1H, Bipy-H4′), 7.88 (t, J = 6.6 Hz, 1H, Bipy-H5), 7.80 (t, J = 6.6 Hz, 1H, Bipy-H5′), 7.54 (d, J = 15.6 Hz, 1H, H6), 7.35 (t, J = 7.8 Hz, 1H, Ar—H5), 7.28 (d, J = 8.4 Hz, H, Ar—H6), 7.27 (s, 1H, Ar—H2), 7.01 (d, J = 7.8 Hz, 1H, Ar—H4), 6.87 (d, J = 15.6 Hz, 1H, H5), 5.86 (s, 1H, H3), 3.81 (s, 3H, OCH_3-3), 2.21 (s, 3H, CH_3). ^{13}C NMR (DMSO-d_6, 150 MHz) δ: 188.65(C-2), 176.93(C-4), 159.54(Ar—C3), 155.39(Bipy-C2), 155.38(Bipy-C2′), 146.98(Bipy-C6), 146.61(Bipy-C6′), 142.02(Bipy-C4), 142.00(Bipy-C4′), 140.92(C-6), 135.97(Ar—C1), 129.90(Ar—C5), 127.91(Bipy-C5), 127.54(Bipy-C5′), 124.23(Ar—C6), 123.99(Bipy-C3), 123.96(Bipy-C3′), 121.06(C-5), 115.98(Ar—C4), 113.19(Ar—C2), 104.03(C-3), 55.18(OCH_3-3), 25.97(C-1). ESI-MS (*m/z*): $[M\text{-}PF_6]^+$ calcd for $C_{23}H_{21}N_2O_3Pd$, 479.0; Found: 479.0. Anal. calcd for $C_{23}H_{21}F_6N_2O_3PPd$: C, 44.21; H, 3.39; N, 4.48. Found: C, 43.92; H, 3.56; N, 4.45%.

*2.2.2.3. Complex **3c***. Yellow solid, Yield: 84%. ^{1}H NMR (600 MHz, DMSO-d_6) δ: 8.58 (d, J = 5.4 Hz, 1H, Bipy-H6), 8.55 (d, J = 6.6 Hz, 1H, Bipy-H6′), 8.54 (d, J = 6.6 Hz, 1H, Bipy-H3), 8.44 (d, J = 5.4 Hz, 1H, Bipy-H3′), 8.40 (t, J = 7.8 Hz, 1H, Bipy-H4), 8.37 (t, J = 7.8 Hz, 1H, Bipy-H4′), 7.90 (t, J = 6.6 Hz, 1H, Bipy-H5), 7.83 (t, J = 6.6 Hz, 1H, Bipy-H5′), 7.69 (d, J = 8.4 Hz, 2H, Ar—H2 and Ar—H6), 7.58 (d, J = 15.6 Hz, 1H, H6), 7.01 (d, J = 8.4 Hz, 2H, Ar—H3 and Ar—H5), 6.73 (d, J = 15.6 Hz, 1H, H5), 5.84 (s, 1H, H3), 3.84 (s, 3H, OCH_3-4), 2.21 (s, 3H, CH_3). ^{13}C NMR (DMSO-d_6, 150 MHz) δ: 187.76(C-2), 177.30(C-4), 161.10(Ar—C4), 155.29 (Bipy-C2 and Bipy-C2′), 146.88 (Bipy-C6), 146.58 (Bipy-C6′), 141.94(Bipy-C4), 141.91(Bipy-C4′), 141.08(C-6), 130.21(Ar—C2 an Ar—C6), 127.84(Bipy-C5), 127.49(Bipy-C5′), 127.14(Ar—C1), 123.89(Bipy-C6′), 123.85(Bipy-C6), 121.24(C-5), 114.34(Ar—C3 an Ar—C5), 103.57(C-3), 55.32(OCH_3-4), 25.78(C-1). ESI-MS (*m/z*): $[M\text{-}PF_6]^+$ calcd for $C_{23}H_{21}N_2O_3Pd$, 479.0; Found: 479.0. Anal. calcd for $C_{23}H_{21}F_6N_2O_3PPd$: C, 44.21; H, 3.39; N, 4.48. Found: C, 43.79; H, 3.20; N, 4.44%.

*2.2.2.4. Complex **3d***. Yellow solid, Yield: 90%. ^{1}H NMR (600 MHz, DMSO-d_6) δ: 8.65 (d, J = 5.4 Hz, 1H, Bipy-H6), 8.60 (d, J = 8.4 Hz, 1H,

Bipy-H6′), 8.58 (d, J = 8.4 Hz, 1H, Bipy-H3), 8.51 (d, J = 4.8 Hz, 1H, Bipy-H3′), 8.44 (td, J_1 = 7.8 Hz, J_2 = 1.2 Hz, 1H, Bipy-H4), 8.41 (td, J_1 = 7.8 Hz, J_2 = 1.2 Hz, 1H, Bipy-H4′), 7.95 (t, J = 6.6 Hz, 1H, Bipy-H5), 7.86 (t, J = 6.6 Hz, 1H, Bipy-H5′), 7.63 (d, J = 15.6 Hz, 1H, H6), 7.33 (d, J = 1.8 Hz, 1H, Ar—H2), 7.31 (dd, J_1 = 7.8 Hz, J_2 = 1.8 Hz, 1H, Ar—H6), 7.01 (d, J = 8.4 Hz, 1H, Ar—H5), 6.85 (d, J = 15.6 Hz, 1H, H5), 5.91 (s, 1H, H3), 3.83 (s, 3H, OCH_3-3), 3.82 (s, 3H, OCH_3-4), 2.26 (s, 3H, CH_3). ^{13}C NMR (DMSO-d_6, 150 MHz) δ: 187.90(C-2), 177.84(C-4), 155.73(Bipy-C2), 155.68(Bipy-C2′), 151.14(Ar—C3), 149.00(Ar—C4), 146.86(Bipy-C6 and Bipy-C6′), 142.10(Bipy-C4 and Bipy-C4′), 141.71(C-6), 127.92(Bipy-C5), 127.56(Bipy-C5′), 124.04(Bipy-C3), 124.02(Bipy-C3′), 123.53(Ar—C1), 121.76 (Ar—C6), 111.54(Ar—C5), 110.18(Ar—C2), 103.62(C-3), 55.60(OCH_3-3 and OCH_3-4), 25.91(C-1). ESI-MS (m/z): $[M\text{-}PF_6]^+$ calcd for $C_{24}H_{23}N_2O_4Pd$, 509.1; Found: 509.1. Anal. calcd for $C_{24}H_{23}F_6N_2O_4PPd$: C, 44.02; H, 3.54; N, 4.28. Found: C, 44.27; H, 3.32; N, 4.39%.

2.2.2.5. Complex ***3e***. Yellow solid, Yield: 95%. ^{1}H NMR (600 MHz, DMSO-d_6) δ: 8.60 (d, J = 4.8 Hz, 1H, Bipy-H6), 8.58 (d, J = 4.8 Hz, 1H, Bipy-H6′), 8.57 (d, J = 4.8 Hz, 1H, Bipy-H3), 8.47 (d, J = 4.8 Hz, 1H, Bipy-H3′), 8.42 (t, J = 7.8 Hz, 1H, Bipy-H4), 8.39 (t, J = 7.8 Hz, 1H, Bipy-H4′), 7.92 (t, J = 6.6 Hz, 1H, Bipy-H5), 7.85 (t, J = 6.6 Hz, 1H, Bipy-H5′), 7.55 (d, J = 15.6 Hz, 1H, H6), 6.93 (d, J = 15.6 Hz, 1H, H5), 6.88 (s, 2H, Ar—H2 and Ar—H6), 6.53 (s, 1H, Ar—H4), 5.92 (s, 1H, H3), 3.78 (s, 6H, OCH_3–3 and OCH_3–5), 2.26 (s, 3H, CH_3). ^{13}C NMR (DMSO-d_6, 150 MHz) δ: 188.83(C-2), 177.17(C-4), 160.66 (Ar—C3 an Ar—C5), 155.63(Bipy-C2), 155.58(Bipy-C2′), 147.21(Bipy-C6), 146.77(Bipy-C6′), 142.05(Bipy-C4 and Bipy-C4′), 141.07(C-6), 136.59 (Ar—C1), 127.89(Bipy-C5), 127.52(Bipy-C5′), 124.68(C-5), 123.99(Bipy-C3 and Bipy-C3′), 106.36 (Ar—C2 and Ar—C6), 104.04(C-3), 102.09 (Ar—C4), 55.32(OCH_3-3 and OCH_3-5), 26.02(C-1). ESI-MS (m/z): $[M\text{-}PF_6]^+$ calcd for $C_{24}H_{23}N_2O_4Pd$, 509.1; Found: 509.1. Anal. calcd for $C_{24}H_{23}F_6N_2O_4PPd$: C, 44.02; H, 3.54; N, 4.28. Found: C, 43.85; H, 3.62; N, 4.30%.

2.2.2.6. Complex ***3f***. Yellow solid, Yield: 83%. ^{1}H NMR (600 MHz, DMSO-d_6) δ: 8.67 (d, J = 5.4 Hz, 1H, Bipy-H6), 8.60 (d, J = 9.0 Hz, 1H, Bipy-H6′), 8.58 (d, J = 9.0 Hz, 1H, Bipy-H3), 8.52 (d, J = 5.4 Hz, 1H, Bipy-H3′), 8.44 (t, J = 8.4 Hz, 1H, Bipy-H4), 8.41 (t, J = 8.4 Hz, 1H, Bipy-H4′), 7.96 (t, J = 6.6 Hz, 1H, Bipy-H5), 7.87 (t, J = 6.6 Hz, 1H, Bipy-H5′), 7.62 (d, J = 15.6 Hz, 1H, H6), 7.07 (s, 2H, Ar—H2 and Ar—H6), 6.94 (d, J = 15.6 Hz, 1H, H5), 5.94 (s, 1H, H3), 3.85 (s, 6H, OCH_3-3 and OCH_3-5), 3.73 (s, 3H, OCH_3-4), 2.28 (s, 3H, CH_3). ^{13}C NMR (DMSO-d_6, 150 MHz) δ: 188.44(C-2), 177.55(C-4), 155.72(Bipy-C2), 155.67(Bipy-C2′), 153.08(Ar—C3 and Ar—C5), 147.31(Bipy-C6), 146.86(Bipy-C6′), 142.11(Bipy-C4), 141.45(Bipy-C4′), 139.61(C-6), 130.30(Ar—C4), 127.97(Bipy-C5), 127.56(Bipy-C5′), 124.06(Bipy-C3), 124.03(Bipy-C3′), 123.57(C-5), 106.04 (Ar—C2 and Ar—C6), 103.89(C-3), 60.14(OCH_3-4), 56.06(OCH_3-3 and OCH_3-5), 25.98(C-1). ESI-MS (m/z): $[M\text{-}PF_6]^+$ calcd for $C_{25}H_{25}N_2O_5Pd$, 539.1; Found: 539.1. Anal. calcd for $C_{25}H_{25}F_6N_2O_5PPd$: C, 43.84; H, 3.68; N, 4.09. Found: C, 43.81; H, 3.72; N, 4.11%.

2.2.2.7. Complex ***3 g***. Yellow solid, Yield: 86%. ^{1}H NMR (600 MHz, DMSO-d_6) δ: 9.66 (s, 1H, Ar-OH), 8.62 (d, J = 4.8 Hz, 1H, Bipy-H6), 8.57 (d, J = 7.8 Hz, 2H, Bipy-H6′ and Bipy-H3), 8.49 (d, J = 4.8 Hz, 1H, Bipy-H3′), 8.42 (t, J = 8.4 Hz, 1H, Bipy-H4), 8.40 (t, J = 8.4 Hz, 1H, Bipy-H4′), 7.91 (t, J = 6.6 Hz, 1H, Bipy-H5), 7.86 (t, J = 6.6 Hz, 1H, Bipy-H5′), 7.59 (d, J = 15.6 Hz, 1H, H6), 7.26 (t, J = 7.8 Hz, 1H, Ar—H5), 7.19 (d, J = 7.8 Hz, 1H, Ar—H6), 7.13 (s, 1H, Ar—H2), 6.87 (dd, J_1 = 7.8 Hz, J_2 = 1.2 Hz, 1H, Ar—H4), 6.82 (d, J = 15.6 Hz, 1H, H5), 5.95 (s, 1H, H3), 2.25 (s, 3H, CH_3). ^{13}C NMR (DMSO-d_6, 150 MHz) δ: 188.54(C-2), 177.05(C-4), 157.71(Ar—C3), 155.46(Bipy-C2), 155.43(Bipy-C2′), 147.01(Bipy-C6), 146.65(Bipy-C6′), 142.03(Bipy-C4), 141.38(Bipy-C4′), 135.95(Ar—C1), 129.84(Ar—C5), 127.89(Bipy-C5), 127.57(Bipy-C5′), 124.03(Bipy-C3), 123.77(Bipy-C3′), 119.49(Ar—C6), 117.54(Ar—C2), 114.76(Ar—C4), 103.85(C-3), 25.97(C-1). ESI-MS (m/z): $[M\text{-}PF_6]^+$ calcd for $C_{22}H_{19}N_2O_3Pd$, 465.0; Found: 465.0. Anal. calcd for $C_{22}H_{19}F_6N_2O_3PPd$: C, 43.26; H, 3.14; N, 4.59. Found: C, 43.37; H, 3.27; N, 4.64%.

2.2.2.8. Complex ***3h***. Yellow solid, Yield: 86%. ^{1}H NMR (600 MHz, DMSO-d_6) δ: 10.13 (br s, 1H, Ar-OH), 8.49–8.50 (m, 3H, Bipy-H6, Bipy-H6′ and Bipy-H3), 8.38 (d, J = 5.4 Hz, 1H, Bipy-H3′), 8.32–8.36 (m, 2H, Bipy-H4 and Bipy-H4′), 7.86 (t, J = 6.6 Hz, 1H, Bipy-H5), 7.80 (t, J = 6.6 Hz, 1H, Bipy-H5′), 7.57 (d, J = 8.4 Hz, 2H, Ar—H2 and Ar—H6), 7.48 (d, J = 15.6 Hz, 1H, H6), 6.84 (d, J = 8.4 Hz, 2H, Ar—H3 and Ar—H5), 6.59 (d, J = 15.6 Hz, 1H, H5), 5.74 (s, 1H, H3), 2.16 (s, 3H, CH_3). ^{13}C NMR (DMSO-d_6, 150 MHz) δ: 187.25(C-2), 177.29(C-4), 159.88(Ar—C4), 155.20(Bipy-C2), 155.17(Bipy-C2′), 146.65(Bipy-C6), 146.48(Bipy-C6′), 141.86(Bipy-C4 and Bipy-C4′), 141.54(C-6), 130.48(Ar—C2 and Ar—C6), 127.80(Bipy-C5), 127.46(Bipy-C5′), 125.63(C-5), 123.87(Bipy-C3), 123.84(Bipy-C3′), 120.08(Ar—C1), 115.84(Ar—C3 and Ar—C5), 103.39(C-3), 25.69(C-1). ESI-MS (m/z): $[M\text{-}PF_6]^+$ calcd for $C_{22}H_{19}N_2O_3Pd$, 465.0; Found: 465.0. Anal. calcd for $C_{22}H_{19}F_6N_2O_3PPd$: C, 43.26; H, 3.14; N, 4.59. Found: C, 43.31; H, 3.26; N, 4.61%.

2.2.2.9. Complex ***3i***. Yellow solid, Yield: 98%. ^{1}H NMR (600 MHz, DMSO-d_6) δ: 9.84 (br s, 1H, Ar-OH-3), 9.21 (br s, 1H, Ar-OH-4), 8.49 (d, J = 8.4 Hz, 1H, Bipy-H6), 8.47 (d, J = 7.8 Hz, 2H, Bipy-H6′ and Bipy-H3), 8.39 (d, J = 4.8 Hz, 1H, Bipy-H3′), 8.34 (t, J = 7.8 Hz, 1H, Bipy-H4), 8.32 (t, J = 8.4 Hz, 1H, Bipy-H4′), 7.86 (t, J = 6.6 Hz, 1H, Bipy-H5), 7.79 (t, J = 6.6 Hz, 1H, Bipy-H5′), 7.41 (d, J = 15.6 Hz, 1H, H6), 7.11 (s, 1H, Ar—H2), 7.05 (d, J = 7.8 Hz, 1H, Ar—H6), 6.80 (d, J = 7.8 Hz, 1H, Ar—H5), 6.50 (d, J = 15.6 Hz, 1H, H5), 5.75 (s, 1H, H3), 2.15 (s, 3H, CH_3). ^{13}C NMR (DMSO-d_6, 150 MHz) δ: 187.08(C-2), 177.34(C-4), 155.30(Bipy-C2), 155.26(Bipy-C2′), 148.58(Ar—C4), 146.70(Bipy-C6), 146.46(Bipy-C6′), 145.60(Ar—C3), 142.06(Bipy-C4), 142.05(Bipy-C4′), 141.83(C-6), 127.76(Bipy-C5), 127.44(Bipy-C5′), 126.19(Ar—C1), 123.89(C-5), 122.08(Ar—C6), 120.05(Bipy-C3), 120.02(Bipy-C3′), 115.66(Ar—C5), 114.75(Ar—C2), 103.31(C-3), 25.70(C-1). ESI-MS (m/z): $[M\text{-}PF_6]^+$ calcd for $C_{22}H_{19}N_2O_3Pd$, 481.0; Found: 481.0. Anal. calcd for $C_{22}H_{19}F_6N_2O_4PPd$: C, 42.16; H, 3.06; N, 4.47. Found: C, 42.19; H, 3.11; N, 4.46%.

2.2.2.10. Complex ***3j***. Yellow solid, Yield: 89%. ^{1}H NMR (600 MHz, DMSO-d_6) δ: 9.46 (s, 2H, Ar-OH-3 and Ar-OH-5), 8.65 (d, J = 5.4 Hz, 1H, Bipy-H6), 8.61 (d, J = 8.4 Hz, 2H, Bipy-H6′ and Bipy-H3), 8.54 (d, J = 6.0 Hz, 1H, Bipy-H3′), 8.45–8.41 (m, 2H, Bipy-H4 and Bipy-H4′), 7.93 (t, J = 6.0 Hz, 1H, Bipy-H5), 7.88 (t, J = 6.0 Hz, 1H, Bipy-H5′), 7.54 (d, J = 15.6 Hz, 1H, H6), 6.75 (d, J = 15.6 Hz, 1H, H5), 6.62 (d, J = 1.8 Hz, 2H, Ar—H2 and Ar—H6), 6.36 (t, J = 1.8 Hz, 1H, Ar—H4), 6.00 (s, 1H, H3), 2.27 (s, 3H, CH_3). ^{13}C NMR (DMSO-d_6, 150MHz) δ: 188.51(C-2), 177.27(C-4), 158.65(Ar—C3 and Ar—C5), 155.58(Bipy-C2), 155.54(Bipy-C2′), 147.12(Bipy-C6), 146.74(Bipy-C6′), 142.03(Bipy-C4 and Bipy-C4′), 141.87(C-6), 136.40(Ar—C1), 127.87(Bipy-C5), 127.55(Bipy-C5′), 124.04(Bipy-C3 and Bipy-C3′), 123.60(C-5), 106.55(Ar—C2 and Ar—C6), 104.90(Ar—C4), 103.73(C-3), 25.96(C-1). ESI-MS (m/z): $[M\text{-}PF_6]^+$ calcd for $C_{22}H_{19}N_2O_3Pd$, 481.0; Found: 481.0. Anal. calcd for $C_{22}H_{19}F_6N_2O_4PPd$: C, 42.16; H, 3.06; N, 4.47. Found: C, 42.19; H, 3.00; N, 4.49%.

2.2.2.11. Complex ***3k***. Yellow solid, Yield: 85%. ^{1}H NMR (600 MHz, DMSO-d_6) δ: 9.79 (br s, 1H, Ar-OH-4), 8.46(d, J = 5.4 Hz, 1H, Bipy-H6), 8.44 (d, J = 7.8 Hz, 1H, Bipy-H6′), 8.43 (d, J = 7.8 Hz, 1H, Bipy-H3), 8.34(d, J = 4.8 Hz, 1H, Bipy-H3′), 8.33(t, J = 7.8 Hz, 1H, Bipy-H4), 8.29 (t, J = 7.8 Hz, 1H, Bipy-H4′), 7.86 (t, J = 6.0 Hz, 1H, Bipy-H5), 7.76 (t, J = 6.0 Hz, 1H, Bipy-H5′), 7.41 (d, J = 15.6 Hz, 1H, H6), 7.23 (s, 1H, Ar—H2), 7.13 (d, J = 8.4 Hz, 1H, Ar—H6), 6.80 (d, J = 8.4 Hz, 1H, Ar—H5), 6.61 (d, J = 15.6 Hz, 1H, H5), 5.70 (s, 1H,

H3), 3.82 (s, 3H, OCH_3-3), 2.14 (s, 3H, CH_3). ^{13}C NMR (DMSO-d_6, 150 MHz) δ: 187.09(C-2), 177.43(C-4), 155.25 (Bipy-C2 and Bipy-C2′), 149.53(Ar—C3), 147.91(Ar—C4), 146.72(Bipy-C6), 146.46(Bipy-C6′), 141.83(C-6), 141.81(Bipy-C4 and Bipy-C4′), 127.79(Bipy-C5), 127.43(Bipy-C5′), 126.15(Ar—C1), 123.89(C-5), 123.83(Bipy-C3 and Bipy-C3′), 120.38(Ar—C6), 115.51(Ar—C5), 110.75(Ar—C2), 103.48(C-3), 55.61(OCH_3-3), 25.71(C-1). ESI-MS (*m/z*): $[M\text{-}PF_6]^+$ calcd for $C_{23}H_{21}N_2O_4Pd$, 495.1; Found: 495.1. Anal. calcd for $C_{23}H_{21}F_6N_2O_4PPd$: C, 43.11; H, 3.30; N, 4.37. Found: C, 43.28; H, 3.24; N, 4.41%.

*2.2.2.12. Complex **3l**.* Yellow solid, Yield: 94%. ^1H NMR (600 MHz, DMSO-d_6) δ: 9.19 (s, 1H, Ar-OH-3), 8.52 (d, J = 5.4 Hz, 2H, Bipy-H6 and Bipy-H6′), 8.51 (d, J = 4.8 Hz, 1H, Bipy-H3), 8.39 (d, J = 5.4 Hz, 1H, Bipy-H3′), 8.37 (t, J = 7.2 Hz, 1H, Bipy-H4), 8.35 (t, J = 7.8 Hz, 1H, Bipy-H4′), 7.88 (t, J = 6.6 Hz, 1H, Bipy-H5), 7.81 (t, J = 6.6 Hz, 1H, Bipy-H5′), 7.46 (d, J = 15.6 Hz, 1H, H6), 7.16 (d, J = 8.4 Hz, 1H, Ar—H6), 7.14 (s, 1H, Ar—H2), 6.97 (d, J = 8.4 Hz, 1H, Ar—H5), 6.59 (d, J = 15.6 Hz, 1H, H5), 5.80 (s, 1H, H3), 3.85 (s, 3H, OCH_3-4), 2.18 (s, 3H, CH_3). ^{13}C NMR (DMSO-d_6, 150 MHz) δ: 187.52(C-2), 177.42(C-4), 155.42(Bipy-C2 and Bipy-C2′), 150.12(Ar—C4), 146.93(Ar—C3), 146.63(Bipy-C6), 146.60(Bipy-C6′), 141.95(Bipy-C4), 141.92(Bipy-C4′), 141.67(C-6), 127.83(Ar—C1), 127.56(Bipy-C5), 127.50(Bipy-C5′), 123.98 (Bipy-C3), 123.95(Bipy-C3′), 121.70(C-5), 121.18(Ar—C6), 114.33(Ar—C2), 111.77(Ar—C5), 103.48(C-3), 55.65(OCH_3–4), 25.83(C-1). ESI-MS (*m/z*): $[M\text{-}PF_6]^+$ calcd for $C_{23}H_{21}N_2O_4Pd$, 495.1; Found: 495.1. Anal. calcd for $C_{23}H_{21}F_6N_2O_4PPd$: C, 43.11; H, 3.30; N, 4.37. Found: C, 43.36; H, 3.25; N, 4.45%.

*2.2.2.13. Complex **3m**.* Yellow solid, Yield: 94%. ^1H NMR (600 MHz, DMSO-d_6) δ: 8.46 (d, J = 7.2 Hz, 2H, Bipy-H6 and Bipy-H6′), 8.44 (d, J = 8.4 Hz, 1H, Bipy-H3), 8.35 (d, J = 7.8 Hz, 1H, Bipy-H3′), 8.33 (t, J = 5.4 Hz, 1H, Bipy-H4), 8.30 (t, J = 7.8 Hz, 1H, Bipy-H4′), 7.85 (t, J = 6.6 Hz, 1H, Bipy-H5), 7.76 (t, J = 6.6 Hz, 1H, Bipy-H5′), 7.41 (d, J = 15.6 Hz, 1H, H6), 7.25 (s, 1H, Ar—H2), 7.18 (d, J = 7.8 Hz, 1H, Ar—H6), 6.93 (d, J = 7.8 Hz, 1H, Ar—H5), 6.64 (d, J = 15.6 Hz, 1H, H5), 6.09 (s, 2H, methylene), 5.71 (s, 1H, H3), 2.15 (s, 3H, CH_3). ^{13}C NMR (DMSO-d_6, 150 MHz) δ: 188.07(C-2), 177.42(C-4), 155.55(Bipy-C2), 155.50(Bipy-C2′), 149.32(Ar—C3), 148.01(Ar—C4), 147.13(Bipy-C6), 146.75(Bipy-C6′), 142.04(Bipy-C4), 142.02(Bipy-C4′), 141.21(C-6), 129.13(Ar—C1), 127.87(Bipy-C5), 127.52(Bipy-C5′), 125.22(C-5), 123.96(Bipy-C3), 123.94(Bipy-C3′), 121.97(Ar—C6), 108.52(Ar—C5), 106.51(Ar—C2), 103.69(C-3), 101.66(methylene), 25.90(C-1). ESI-MS (*m/z*): $[M\text{-}PF_6]^+$ calcd for $C_{23}H_{19}N_2O_4Pd$, 493.1; Found: 493.2. Anal. calcd for $C_{23}H_{19}F_6N_2O_4PPd$: C, 43.25; H, 3.00; N, 4.39. Found: C, 43.48; H, 2.97; N, 4.47%.

2.3. Cytotoxic activity

2.3.1. Cell lines and culture

Human cancer cell lines (HeLa, MCF-7 and MGC803) were grown in DMEM supplemented with 10% of FBS, 100 IU/mL penicillin and 100 μg/mL streptomycin, in the presence of 5% CO_2 under normal culture conditions (37 °C, absolute humidity). All the experiments have been performed at the earlier passage of the cell lines.

2.3.2. MTT assay

The MTT assay was used to determine the cytotoxicity of all the complexes on HeLa, MCF-7 and MGC803 cancer cell lines. 1.5×10^4 Cells per well of cancer cells were seeded into 96-well plates and incubated under standard condition for 24 h. After removing the medium, the cells were then exposed to various concentrations of the palladium complexes and cisplatin, and incubated for 48 h. When necessary, pretreatment with *N*-acetylcysteine (NAC) for 1 h was conducted before adding test complex. After incubation with 10 μL of MTT for 4 h, the medium was removed and replaced by 100 μL of dimethyl sulfoxide (DMSO). The optical density (OD) value was read at 570 nm using a multiwell plate reader.

2.4. Measurement of reactive oxygen species (ROS)

1.5×10^5 Cells per well of HeLa cells were seeded in 6-well plates and treated with increasing concentrations (5 μM, 10 μM and 20 μM) of complex **3e** for 24 h. Subsequently, cells were detached and incubated with 20 μM of DCFH-DA in phosphate-buffered saline. Relative fluorescence intensity of 2′,7′-dichlorofluoroscein (DCF) was measured at excitation and emission wavelengths of 488 nm and 525 nm by a flow cytometer. To confirm the effect of intracellular ROS on the cells, 2 mM NAC was treated for 1 h before complex **3e** treatment. After incubation with ROS scavengers and/or complex **3e** for 24 h, the cells were collected for further analyses.

2.5. Cell apoptosis analysis

The ability of complex **3e** to induce apoptosis was evaluated in HeLa cells line by flow cytometry, using Annexin V conjugated with fluorescein isothiocyanate (FITC) and propidium iodide (PI) counterstaining. In a 6-well culture plate, 1.5×10^5 HeLa cells with 2 mL culture medium were seeded and incubated for 12 h. Then the medium containing complex **3e** was added. After 24 h incubation, cells were collected, washed twice with cold PBS (pH 7.4, 100 μg/mL) and then suspended in 400 μL Binding Buffer. 5 μL of Annexin V-FITC were added. After gentle vortexing, the cells were incubated for 15 min at 2–8 °C, in the dark. And then 10 μL PI were added, incubated for 5 min at 2–8 °C, in the dark and analyzed by flow cytometry within 1 h.

2.6. Cell cycle analysis

HeLa cells (1.5×10^5/mL) in DMEM medium with 10% FBS were seeded into 6-well plates and the final volume is 2 mL. After 24 h of incubation, cells were further incubated with different concentrations complex **3e** for another 24 h. Then cells were treated and analyzed by flow cytometry as previously described [43]. The ModFit software was utilized to analyse the corresponding cell cycle distribution.

2.7. Measurement of mitochondrial membrane potential

The mitochondrial potential was assessed by using the JC-1 dye. Briefly, 1.5×10^5 cells (HeLa) were cultured in 6-well plate overnight at 37 °C, and then treated with different concentrations of complex **3e** for 24 h. Meanwhile, cells served as a positive control were treated with *m*-chlorophenylhydrazone (CCCP) for 30 min at 37 °C. The medium was then removed and the cells were trypsinized, collected and pellets formed at 2000 rpm. All the treated cells were then stained with the JC-1 dye for 20 min at 37 °C. The pellets were resuspended in PBS (1 mL). The fluorescence of JC-1 was determined by flow cytometric analysis with excitation at 488 nm and emission at 530 nm (FL1 channel, for JC-1 monomer) and 580 nm (FL2 channel, for aggregates of JC-1).

2.8. Interaction of CT-DNA with complex **3e**

2.8.1. UV–vis spectroscopy

Stock solutions of CT-DNA were prepared according to the reported method and incubated at 4 °C for 12 h [56]. The concentration of CT-DNA solution was 2.5 mM, determined by UV absorbance at 260 nm. The ratio (1.8–1.9) of UV absorbance at 260 and 280 nm of DNA solution indicated that DNA was free of protein. The complex solution was prepared by mixing the DMSO solution of **3e** and Tris-HCl buffer (pH = 7.2) and the final concentration of complex **3e** was 10 μM. To prepare series of complex-DNA solutions, certain amount of DNA stock solution (2.5 mM) was added to the above solution of complex **3e**. The

corresponding electronic absorption spectra were recorded from 200 to 600 nm at room temperature.

2.8.2. Fluorescence spectroscopy

To prepare DNA-EB solution, 25.0 mM ethidium bromide (EB) and 2.5 mM CT-DNA were mixed in 10 mM Tris-HCl buffer solution (pH = 7.2), and the final concentration of EB and CT-DNA maintained at 4.0 and 80.0 μM, respectively. With the addition of certain amount of complex **3e** solution into the prepared DNA-EB solution, fluorescence quenching spectra were recorded using a spectrofluorimeter with an excitation wavelength of 522 nm and emission spectrum of 550–630 nm.

2.8.3. Viscosity measurements

Ubbelodhe viscometer was used in the viscosity measurement experiment and a constant temperature of 30.0 ± 0.1 °C was maintained through a thermostated water-bath. To minimize the complexities arising from DNA flexibility, CT-DNA sample solutions were prepared under the assistance of sonication. Each sample was measured at least three times. Flow time was measured with a digital stopwatch and an average flow time was calculated by three replicated measurements. The relative viscosity was calculated according to the relation $\eta = (t - t_0)/t_0$, where t is the observed flow time for DNA in the presence and absence of the complex and t_0 is the flow time for the buffer [57]. Data were reported as $(\eta/\eta_0)^{1/3}$ versus binding ratio ([complex **3e**]/[DNA]), where η is the viscosity of DNA in the presence of complex **3e** and η_0 is the viscosity of DNA solution alone.

2.9. BSA binding studies

2.9.1. Tryptophan quenching experiment

Tryptophan fluorescence quenching experiment was used to study the protein binding ability of complex **3e**. 1.5 μM BSA solution was prepared by dissolving 10 mg of BSA in 10 mL PBS buffer solution (10 mM, pH 7.4). By keeping the concentration of BSA constant while varying the concentration of complex **3e**, the quenching of the emission intensity of tryptophan residues from BSA at 352 nm was monitored. Fluorescence spectra were recorded from 300 to 450 nm at an excitation wavelength of 285 nm.

2.9.2. Site marker-competitive binding experiments

The site-competitive binding experiments were conducted by adding complex **3e** to a BSA-site marker system. The concentrations of BSA solution were fixed at $5.0 \times 10^{-6}\,M^{-1}$, and the concentrations of complex **3e** varied from 0 to $3.0 \times 10^{-5}\,M^{-1}$ at increments of $2.0 \times 10^{-6}\,M^{-1}$. Fluorescence spectra were measured at 298 K in the range of 300–450 nm at the excitation wavelength of 295 nm.

2.10. Thioredoxin reductase (TrxR) inhibition assay

The TrxR-inhibitory activities of complex **3e** and compound **2e** were examined by a thioredoxin reductase colorimetric assay kit (Solarbio Science & Technology, Beijing, China) followed the manufacturer's instructions.

3. Results and discussion

3.1. Synthesis and characterization

A family of hispolon and its analogs containing peripheral substituents on the aromatic rings were prepared by a procedure reported previously in the literature [58,59]. (Bipy)$PdCl_2$, obtained from the reaction of 2,2′-bipyridine with palladium chloride in acetonitrile, was further treated with silver nitrate to give (bipy)$Pd(ONO_2)_2$ as light yellow solid [60]. As shown in Scheme 2, the combination of a metal-ligand coordination reactions of hispolon related ligands with (bipy)Pd

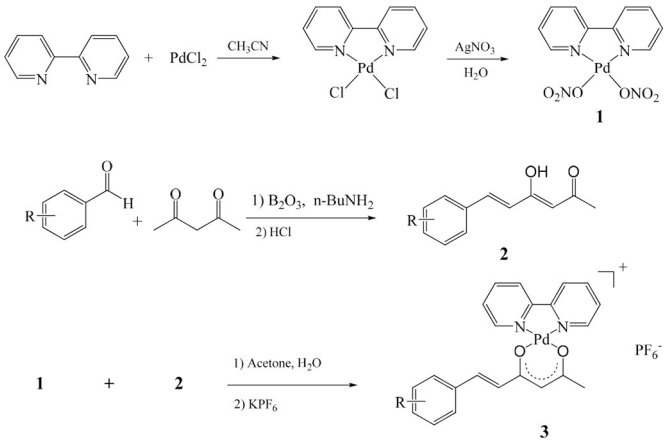

Scheme 2. Synthetic routes for complexes **3a-3m**

$(ONO_2)_2$ in aqueous acetone solution and subsequent anion exchange with KPF_6 yielded the desired cationic palladium(II) complex as hexafluorophosphate salts in excellent yield.

The obtained complexes have been fully characterized by nuclear magnetic resonance (^{1}H NMR and ^{13}C NMR), electrospray ionization mass spectrometry (ESI-MS) and elemental analysis. In the ^{1}H NMR spectra of these complexes, the disappearance of the signal assigned to the enol hydrogen atom (δ = 15.30–15.50 ppm) and the proportion of aromatic protons of (bipy) Pd to a β-diketonate anion indicate the occurrence of spontaneous deprotonation of β-diketonate ligands and the formation of a single product. Generally, two "parts" corresponding to the bipyridine ligand and β-diketone ligand were observed in ^{1}H NMR-spectra of the synthesized palladium(II) complexes. The proton peaks of the bipyridine ligand appeared in the low field at 8.67–7.76 ppm, and that of β-diketone ligand appeared in the high field at 7.80–2.14 ppm except the phenol-OH proton peaks (9.06–10.13 ppm). It is worthwhile to note that all of the complexes exhibit two sets of characteristic doublet with coupling constant of 15.6 Hz, which demonstrate the existence of *E*-configured double bond moiety. Additionally, due to their different symmetry properties, the bipyridine ligand of these complexes showed four sets of doublet and four sets of triplet, different from that of the precursor complex (bipy)$Pd(ONO_2)_2$, which showed only two sets of doublet and two sets of triplet (see ESI).

To further confirm the NMR peaks observed in the ^{1}H and ^{13}C NMR spectra of these complexes, the 2D correlation diagrams HSQC (heteronuclear single-quantum correlation) and HMBC (heteronuclear multiple-bond correlation) spectra of complex **3e** were conducted. The observed HSQC cross-peaks of the carbon and hydrogen (26.02/2.26, 104.04/5.92, 124.68/6.93, and 141.07/7.55) indicate the relationships between hydrogens 1, 3, 5 and 6 with the four key carbon signals (C-1, C-3, C-5 and C-6), respectively. HMBC signals from H-1 to C-2/C-3, H-3 to C-1/C-2/C-4/C-5 and H-5 to C-3/C-4/C-6/Ar-C-1 further solidified the aboved assignments, and the other two key carbon signals 188.80(C-2) and 177.14(C-4) were also determined. Additionally, cross-peaks such as 55.32/3.78, 102.09/6.53 and 106.36/6.88 in the HSQC spectra were also observed, which indicated the presence of a 1,3,5-trisubstituted aromatic ring. HMBC signals from Ar-H-2 (Ar-H-6) to Ar-C-1/Ar-C-3(Ar-C-5)/Ar-C-4 and Ar-H-4 to Ar-C-2(Ar-C-6)/Ar-C-3(Ar-C-5) were also in agreement with the proposed assignments. As 2, 2′-bipyridine moiety in complex **3e**, the combination of HSQC and HMBC further modified the peaks assignment from 1D ^{1}H and ^{13}C NMR methods. As a consequence, all the NMR spectra patterns strongly suggest the existence of mononuclear palladium(II) complex constructed by unsymmetric β-diketonate anion and 2, 2′-bipyridine in solution. The assignments of **3a-3m** as $[Pd(bipy)(O,O'\text{-dkt})]^+$ type complexes in the ESI-MS spectra are also verified by the appearance of the characteristic singly-charged cation $[M\text{-}PF_6]^+$. Elemental analyses

Table 1
In vitro cytotoxicity (IC_{50} values, 48 h) of the ligand (**2a**-**2m**) and cisplatin toward HeLa, MCF-7 and MGC803 cell lines.

Compounds	IC_{50} (μM)		
	HeLa	MCF-7	MGC803
2a	45.20 ± 1.90	60.90 ± 2.94	51.62 ± 1.43
2b	43.18 ± 1.71	> 100	64.91 ± 1.56
2c	> 100	> 100	> 100
2d	55.33 ± 1.89	> 100	51.71 ± 1.77
2e	41.23 ± 1.93	54.80 ± 1.64	53.95 ± 1.59
2f	51.74 ± 1.94	111.30 ± 1.88	56.86 ± 1.79
2 g	44.11 ± 1.45	82.50 ± 1.78	42.09 ± 1.94
2 h	52.20 ± 1.32	> 100	44.04 ± 1.57
2i	111.82 ± 1.36	> 100	> 100
2j	28.10 ± 1.18	40.80 ± 1.27	57.84 ± 1.74
2k	59.05 ± 2.27	> 100	58.11 ± 1.79
2l	59.12 ± 1.57	> 100	57.84 ± 2.13
2m	> 100	> 100	69.31 ± 1.25
Cisplatin	13.64 ± 1.79	20.23 ± 1.37	16.87 ± 1.54

of **3a**-**3m** were found to be completely consistent with the proposed molecular formulas.

3.2. Cancer cell growth inhibition

The cytotoxicity of hispolon analogs and their corresponding palladium(II) complexes was determined using MTT assay (MTT = 3-(4,5-dimetyl-2-thiazolyl)-2,5-diphenyl-2*H*-tetrazolium bromide) on three human cancer cell lines, including HeLa, MCF-7 and MGC803. The IC_{50} values are shown in Tables 1 and 2 and cisplatin was selected as positive control.

As shown in Tables 1 and 2, in addition to the comparable cytotoxicity showed by hispolon and its palladium complex, most of the obtained palladium(II) complexes exhibited stronger cytotoxicity than their ligands alone. And the preliminary results also showed that most of the obtained complexes were to be more toxic against HeLa than MCF-7 and MGC803 cells. Importantly, complex **3e** exhibited more potent cytotoxicity than cisplatin (8.59 μM versus 13.64 μM). The structure-activity relationships (SAR) observed in this study demonstrated that the substituents on the phenyl ring of hispolon analogs played a very important role in activity. On the whole it seems that introduction of methoxy group on the phenyl ring could increase the cytotoxicity and introduction of hydroxyl group on the phenyl ring could reduce the cytotoxicity. These observations are generally consistent with our previous research result on palladium complex of curcumin derivatives [43]. For example, complexes **3b**, **3c**, **3d** and **3e** displayed stronger cytotoxic activity than complexes **3g**, **3h**, **3i** and **3j**. The improved cytotoxicity of the palladium complex with hispolon analog ligand decorated with methoxy group maybe due to their higher lipophilicity than their counterpart with hydroxyl group [44]. The obtained results may be helpful for designing new anticancer drugs in the future.

Table 2
In vitro cytotoxicity (IC_{50} values, 48 h) of the palladium(II) complexes (**3a**-**3m**) and cisplatin toward HeLa, MCF-7 and MGC803 cell lines.

Complexes	IC_{50} (μM)		
	HeLa	MCF-7	MGC803
3a	13.38 ± 1.11	24.34 ± 1.98	26.28 ± 1.90
3b	16.83 ± 1.63	23.12 ± 1.45	20.66 ± 0.95
3c	19.26 ± 1.74	21.51 ± 1.69	21.25 ± 1.58
3d	9.42 ± 1.90	19.86 ± 1.39	18.75 ± 1.90
3e	8.59 ± 1.58	17.88 ± 1.40	14.54 ± 3.12
3f	21.31 ± 1.50	35.64 ± 1.87	21.27 ± 1.77
3g	31.05 ± 1.93	26.25 ± 1.37	22.25 ± 1.56
3h	37.03 ± 1.87	39.52 ± 1.99	82.48 ± 1.45
3i	> 100	99.13 ± 1.85	98.92 ± 1.48
3j	12.84 ± 1.47	> 100	33.41 ± 1.97
3k	40.55 ± 1.66	> 100	91.01 ± 1.93
3l	80.44 ± 0.97	67.65 ± 1.74	74.51 ± 1.57
3m	15.86 ± 2.10	22.46 ± 1.66	21.02 ± 1.38
Cisplatin	13.64 ± 1.64	20.23 ± 1.19	16.87 ± 1.40

3.3. Flow cytometric analysis of apoptosis

Induction of apoptosis in malignant cells is very important for cancer therapy [61]. The Annexin V-FITC/PI double labeling method was used to evaluate the role of apoptosis in complex **3e**-induced HeLa cells death by flow cytometry. As shown in Fig. 1, compared to spontaneous apoptosis of control cells, the values of the early apoptotic phase had a significant increase when HeLa cells were treated with various concentration of complex **3e** for 24 h (Control: 3.59%; 5 μM: 7.78%, 10 μM: 26.05; 20 μM: 71.28%, respectively). It was also found that the apoptotic cells accumulated in a dose-dependent manner from 17.28% to 98.01%. These results demonstrate that complex **3e** actually induced apoptosis of HeLa cells.

3.4. Intracellular ROS accumulation

It's widely accepted that ROS in cancer cells play a central role in regulating and inducing cell apoptosis, and selective modulating ROS maybe represent a promising strategy to kill cancer cells or even multidrug resistant (MDR) cancer cells [62]. At the same time, some palladium(II) complexes with modified curcumin ligands have exhibited excellent prooxidative ability [43]. Based on the above consideration, we further employed the oxidation-sensitive probe, DCFH-DA to measure the intracellular ROS levels by flow cytometry. Catalyzed by intracellular esterase, DCFH-DA could be deacetylated and converted to non-fluorescent DCFH, which was further oxidized to a fluorescent compound DCF by ROS. From the fluorescence intensity of DCF, the amount of ROS produced by the cells could be evaluated [63].

The ROS levels of HeLa tumor cells hatched in complex **3e** (5 μM, 10 μM and 20 μM) were detected by flow cytometry. As shown in Fig. 2, complex **3e**-induced generation of the ROS in a concentration-dependent manner was observed. More importantly, the maximum ROS accumulation with a 2.1-fold increase relative to the control was observed after treatment with 10 μM of complex **3e** for 24 h. It was also found that pretreatment of *N*-acetylcysteine (NAC), the ROS scavenger, significantly inhibited **3e**-induced ROS generation in HeLa cells.

To further elucidate whether ROS generation is directly associated with **3e**-elicited cytotoxicity in HeLa cells, cells were pretreated with NAC for 1 h, and then exposured to **3e** at the indicated concentrations (5 μM, 10 μM, and 20 μM). As expected, NAC significantly attenuated the cytotoxicity (Fig. 3). Taken in concert, the above results further emphasize that the ROS-generating ability of **3e** may be responsible for its better cytotoxicity and apoptosis-inducing activity.

3.5. Effect of complex on mitochondrial membrane potential ($\Delta\Psi_{mit}$)

Mitochondria are the primary source of cellular ROS. As a pro-apoptotic stimulus, ROS may trigger the opening of mitochondrial permeability transition (MPT), which in turn leads to the loss of the mitochondrial transmembrane potential ($\Delta\Psi_{mit}$). $\Delta\Psi_{mit}$ is often considered as an indicator of apoptosis [64]. To determine the values of $\Delta\Psi_{mit}$, the change of JC-1 (a frequently-used fluorescent probe) in HeLa cells inducted by different concentration (5 μM, 10 μM and 20 μM) of complex **3e** was monitored by flow cytometry and fluorescence microscopy. It's well known that the JC-1 dye can accumulate in mitochondria in a potential-dependent manner, characterized by a special shift from green (~529 nm) to red (~590 nm). Consequently, mitochondrial depolarization is indicated by a decrease in the red/green fluorescence intensity ratio. As shown in Fig. 4, complex **3e**-mediated

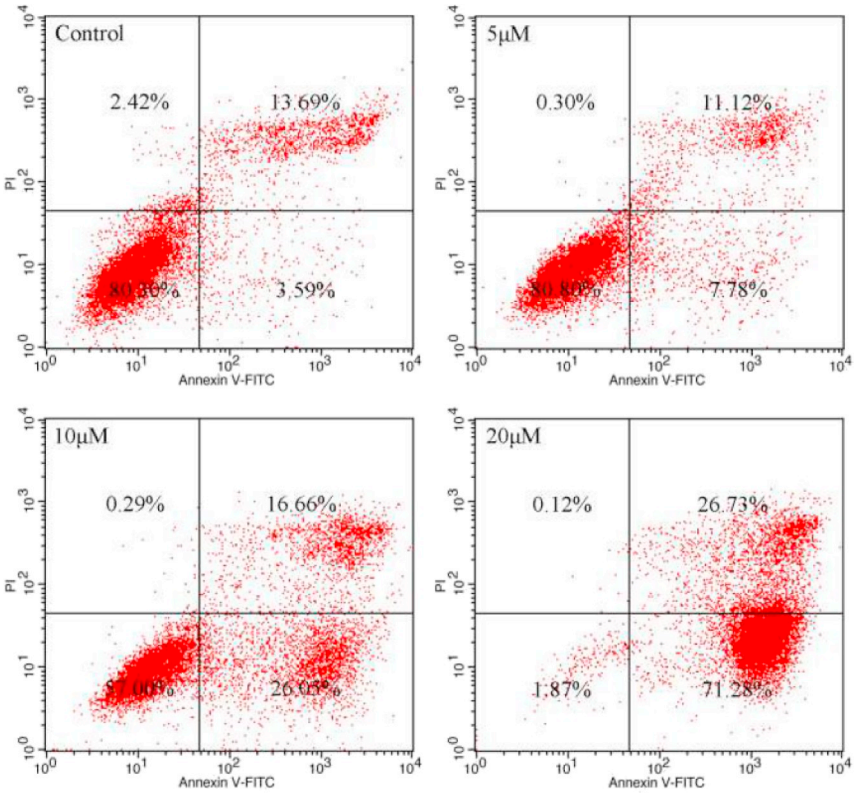

Fig. 1. Apoptosis of HeLa cells was analyzed by flow cytometry after treatment with complex **3e** (5 μM, 10 μM and 20 μM) and annexin V-FITC and PI stained for 24 h. Similar results were obtained in three independent experiments.

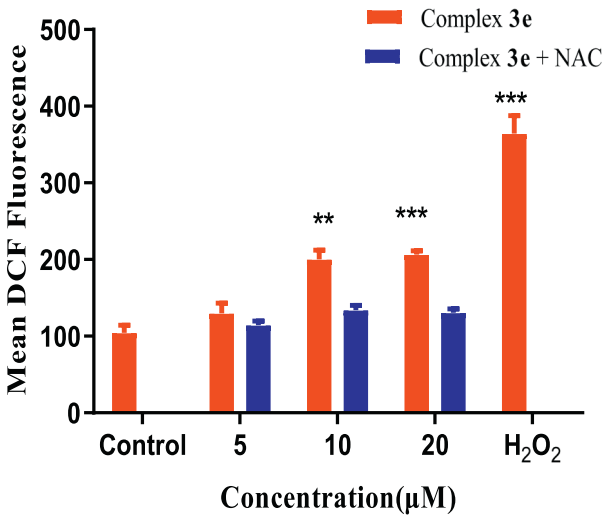

Fig. 2. ROS level in Hela cells treated with complex **3e** for 24 h in presence and absence of the NAC.

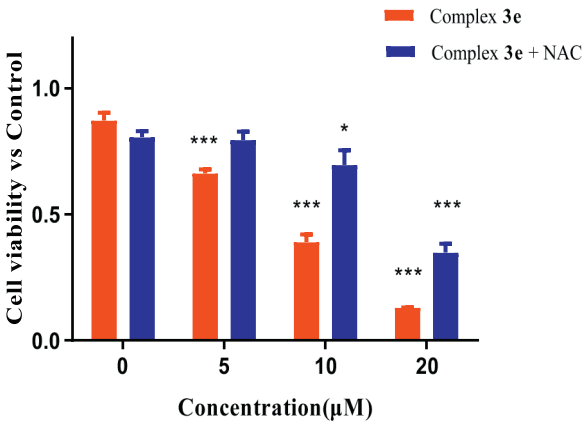

Fig. 3. Cell viability of Hela cells treated with complex **3e** for 48 h in presence and absence of NAC.

significant decrease in a concentration-dependent manner in the $\Delta\Psi_{mit}$ was observed, indicating the impaired mitochondrial integrity and the dysfunction of mitochondria membrane potential.

3.6. Effect of complex on the cell cycle in Hela cells

Cell cycle control represents a major regulatory mechanism for cell growth [65], and it was reported that increase in ROS can reduce cancer cells proliferation by inducing cell cycle arrest [66,67]. To examine the possible relationship between the cytotoxic activity and cell cycle arrest of complex **3e**, cell cycle analysis with propidium iodide (PI) staining by flow cytometry was performed. As shown in Fig. 5, the changes of cell cycle for HeLa cells induced with variable concentrations of complex **3e** (5 μM, 10 μM and 20 μM) were detected after 24 h. As shown, the cell population in G0/G1 phase were reduced from 47.78% to 35.91% after complex **3e** treatment, in association with the increased cell population in the G2/M phase (from 16.11% to 31.06%), and slight changes were observed in the S phase (from 36.41% to 33.03%). The obtained results confirmed that complex **3e** treatment mainly induced the accumulation of cells in the G2/M phase in a dose-dependent manner, and achieving the purpose of apoptosis. To further explore the possible mechanism of cell cycle arrest caused by complex **3e**, western blot was applied to detect the expression of cdc2, the G2/M-related protein. As shown in Fig. S1 (ESI), the upregulation of the levels p-cdc2 was observed, accompanied with slight downregulation of the levels of cdc2. Therefore, the mechanism should be complex **3e** induces ROS in

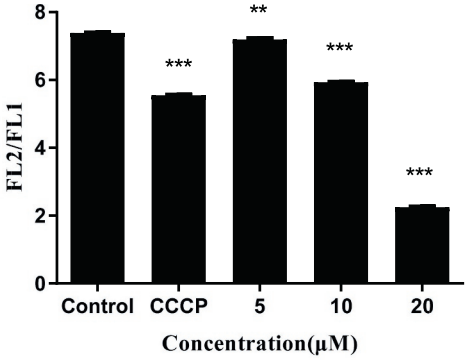

(A)

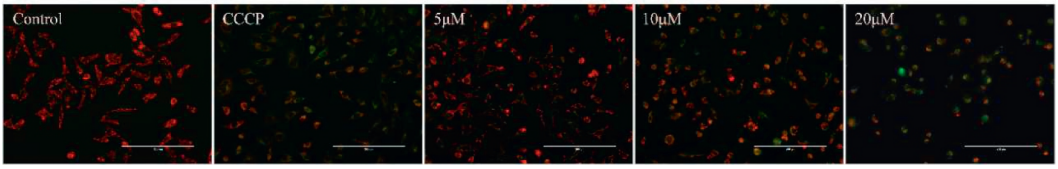

(B)

Fig. 4. Analysis of MMP in HeLa cells treated with complex **3e** at 5 μM, 10 μM and 20 μM for 24 h. (A) The change of MMP was measured with the mitochondria-selective dye JC-1 by flow cytometry. (B) The images were observed with fluorescence microscope (Bar = 200 μm).

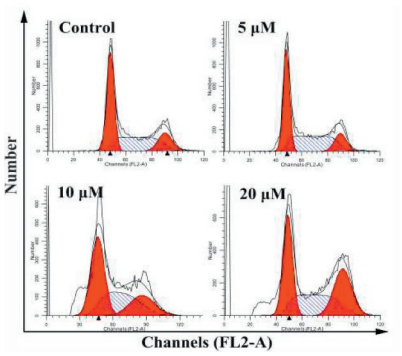

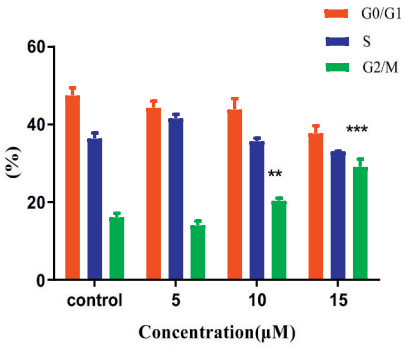

Fig. 5. Effect of complex **3e** (5 μM, 10 μM and 20 μM) on the cell cycle distribution in HeLa cells as estimated by PI staining: (A) representative figure shows distribution of cells in different phase of cell cycle (G0/G1, S, and G2/M) at 48 h after treatment with complex **3e** (B) bar graph shows the percentage (%) of cells in different phases of cell cycle ($^{**}p \leq 0.05$ and $^{***}p \leq 0.001$ compared with control group). Results are presented as average of three independent experiments.

HeLa cells, which leads to cdc2 phosphorylation, resulting the G2/M arrest.

*3.7. Interaction of complex **3e** with CT-DNA by UV–vis titration, fluorescence quenching method and viscosity measurement*

Based on the consideration that DNA is believed to be the primary target for many metal-based drugs, UV–vis absorption spectra, fluorescent spectra and viscosity measurements were utilized to study binding modes of the obtained complex with CT-DNA. Complexes binding with DNA through intercalation generally results in hypochromicity and bathochromic shift in the UV–vis absorption spectra, since the involved strong stacking interaction between the planar aromatic chromophore and the base pairs of DNA [68,69]. Fig. 6 shows the absorption spectra of **3e**, the efficient cytotoxic among complexes, in the presence of increasing amounts of CT-DNA. As shown, there were only apparent decreases in the peak intensities, but being no significant red-shift. Besides, according to the reported equation (Eq. (S1), ESI), the binding constant (K_b) of complex **3e** to CT-DNA was calculated and found to be $6.5 \times 10^4\,M^{-1}$, which is considerably $< 5.0 \times 10^6\,M^{-1}$ reported for the well-known metallo-intercalator $[Ru(bpy)_2(dppz)]^{2+}$ [70]. The calculated K_b, together with the aboved spectral

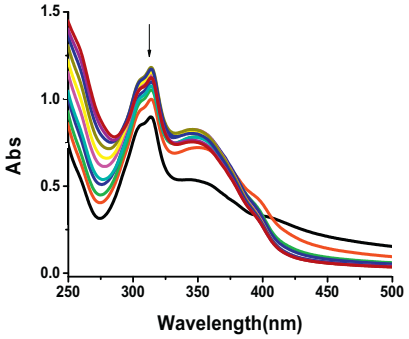

Fig. 6. Absorption spectra of complexes **3e** in the absence and presence of increasing concentration of CT-DNA at room temperature in Tris-HCl (pH = 7.2). The arrow shows the absorbance changes with the concentration of CT-DNA increasing.

characteristics, may suggest that there exist some interactions between complex **3e** and DNA, however, the classical intercalation binding mode should be ruled out in this case.

In order to gain more insights into the binding mode of complex **3e**

with CT-DNA, competitive binding studies with ethidium bromide (EB) bound DNA was carried out. Due to its strong intercalation between the adjacent DNA base pairs, EB usually emits intense fluorescent light in the presence of DNA. The enchanced fluorescence of EB could be quenched by the addition of a compound capable of preventing intercalation of EB to DNA [71]. Based on the fact that EB intercalates DNA through interactions with the minor groove, it is reasonable that an intercalative or minor groove binding mode of a compound with DNA may be deduced from an analysis of ethidiun bromide displacement assay [72–74]. The emission spectra of the EB-DNA system in the absence and presence of increasing amounts of complex **3e** is shown in Fig. S2 (ESI) The significant decrease in intensity of the emission band at 612 nm was observed with the increase of concentration of complex **3e**. This clearly indicates that complex **3e** compete with EB in binding to DNA. The quenching ability is evaluated by the Stern-Volmer quenching constant (K_{sv}).

$$F_0/F = 1 + K_{sv}\,[Q]$$

where F_0 and F are the fluorescence emission intensities in the absence and presence of complex, K_{sv} is the quenching constant, and [Q] is the concentration of complex. From the Stern-Volmer plots (Fig. S2, ESI) of F_0/F versus [Q], the quenching constants $K_{sv} = 1.87 \times 10^4\,M^{-1}$ was obtained for **3e**, suggesting possible groove binding mode of interaction between complex **3e** and CT-DNA [75]. And considering the non-intercalating property of the two chelating ligands and the square-planar configuration of complex **3e** [76,77], a minor-groove binding mode rather than intercalation between complex **3e** and DNA has to be considered, which is consistent with the results obtained from UV–Vis analysis.

To clarify further complex-DNA interaction between intercalation and minor groove binding, the effect of complex **3e** on the relative viscosity of CT-DNA were performed. Fig. S3 (ESI) shows the changes in viscosity upon addition of varying amount of complex **3e**. The results show that the relative viscosity of DNA solution is increased, but the extent of the viscosity increase caused by complex **3e** is considerably lower than that reported for $[Ru(bpy)_2(dppz)]^{2+}$ [70]. It is well known that classical intercalation or the binding with the phosphate group of DNA backbone may cause an increase in the viscosity of DNA solution [57,75,78]. Therefore, electrostatic interaction of positively-charged complex **3e** with phosphate group in the DNA backbone may be also favorable for the minor groove binding. Taken in concert, the above results further reveal that the palladium (II) complex **3e** could interact with DNA through minor groove binding and/or electrostatic interactions.

3.8. Interaction with BSA and the determination of complex-binding site on BSA

Human serum albumin (HSA), the most abundant protein in human blood plasma, plays an important role in many physiological functions. To some extent, the interaction of drugs with HSA maybe greatly affects their transport, delivery, and efficiency [79]. Considering the high structural homology with HSA and its available and affordable property, bovine serum albumin (BSA) is used as the model protein to evaluate the albumin-binding ability of the obtained complexes.

The emission spectra of BSA in the absence and presence of the selected complex **3e** are depicted in Fig. S4 (ESI). In the absence of a drug, a strong emission band at 350 nm (excitation wavelength fixed at 285 nm) was observed. When a fixed concentration of BSA was titrated with various concentration of complex **3e**, the intrinsic fluorescence emission intensities of BSA remarkably decreased, indicating the binding of complex **3e** to albumin. The fluorescence quenching data were further analyzed with the Stern-Volmer equation (Eq. (S2), ESI), and the quenching constant K_{sv} and quenching rate constant k_q were obtained and listed in Table 3. The binding constant K_b and number of binding site n were further calculated by Scatchard equation (Eq. (S3), Fig. S1, ESI). Among these, the value of k_q of complex **3e** was found to be $1.44 \times 10^{12}\,M^{-1}\,s^{-1}$, which was almost two orders of magnitude higher than that of a pure dynamic quenching mechanism ($2.0 \times 10^{10}\,M^{-1}\,s^{-1}$) [80]. This result indicates that static quenching mechanism is the main way for complex **3e** acting on BSA, which may be attributed to the formation of a ground state complex of the type of BSA-complex as has been reported previously [81]. Further, the value of K_b obtained in the this study is comparable with that of mononuclear palladium(II) complexes reported earlier ($10^4\,M^{-1}$) [69,82], but smaller than that of dinuclear and trinuclear palladium(II) complexes ($10^5\,M^{-1}$) [68,83]. The obtained value of n is close to 1, which suggests the existence of single class of binding sites for complex **3e**.

Table 3
The values of K_{sv}, k_q, K_b and n for complex **3e** at 298 K.

Complex	K_{sv} ($10^4\,M^{-1}$)	k_q ($M^{-1}\,s^{-1}$)	K_b (M^{-1})	n
3e	1.44 ± 0.21	1.44×10^{12}	3.58×10^4	1.31

To determine the binding site of complex **3e** on BSA, the site marker competitive experiments were conducted, in which specifical markers bind to a known site or region on BSA were used. Sudlow I and Sudlow II, located in in sub-domains IIA and IIIA, are the common binding sites of BSA [84,85]. It is reported that warfarin binds to the sub-domain IIA (Sudlow's site I) and ibuprofen binds to the sub-domain IIIA (Sudlow's site II) [86]. The information of the binding site on BSA can be obtained by monitoring the changes of the fluorescence of BSA-site marker system with titration of complex **3e** [87,88, Fig. S5 (ESI)]. The binding constants of complex **3e** to BSA in the presence and absence of site markers were calculated and compared. The obtained binding constants in the presence of ibuprofen and warfarin are $7.46 \times 10^3\,M^{-1}$ and $3.02 \times 10^4\,M^{-1}$ at 298 K, while that of just the complex-BSA system is about $3.58 \times 10^4\,M^{-1}$. Obviously, the binding constant in the presence of ibuprofen is much smaller than that in its absence, while that for warfarin is almost the same as without it. These reveal that the competition between complex **3e** and ibuprofen or warfarin is quite similarly, and complex **3e** mainly competes with ibuprofen in sub-domain IIIA (Sudlow's site II). The results clearly indicate that complex **3e** mainly binds to BSA in Sudlow's site II.

3.9. Enzyme inhibition

Based on the above DNA/BSA interactions, it is worth noting that although complex **3e** could bind to DNA, but its relative strong cytotoxicity aroused by ROS may not totally be ascribed to its DNA binding ability. Some proteins involved in ROS generation could not be ruled out in this case. Considering the mammalian thioredoxin reductase (TrxR)-inhibitory activity of hispolon and its derivatives [55], we speculate that TrxR may be the possible target. To prove it, TrxR assay was conducted and the TrxR-inhibitory activity of complex **3e** was quantified by the change in absorbance at 412 nm of 5,5′-dithiobis-2-nitrobenzoic acid (DTNB) to thionitrobenzoic acid [89]. It was found that the TrxR-inhibitory activity of complex **3e** is comparable with that of a palladium complex with thiosemicarbazone ligand reported in the literature [90], and was about 5-fold more potent than that of compound **2e** [Table 4]. More work needed to support the potential of the obtained palladium(II) complexes as TrxR inhibitors are undergoing in our laboratory.

Table 4
IC_{50} values of compounds for TrxR inhibition.

Compounds	Enzyme inhibition (IC_{50}, μM)
2e	39.17 ± 1.59
3e	8.38 ± 0.92

4. Conclusion

In this paper, a family of palladium(II) complexes with hispolon analogs were designed, synthesized and characterized by ^{1}H (^{13}C) NMR, ESI-MS and elemental analysis. The obtained complexes manifested significant in vitro cytotoxic activity against three different human cancer cell lines, such as HeLa, MCF-7 and MGC803. Importantly, four palladium(II) complexes (**3b**, **3c**, **3d** and **3e**) with methoxyl-decorated hispolon analog ligand exhibit enhanced antitumor activity than those (**3g**, **3h**, **3i** and **3j**) with hydroxyl-decorated hispolon analog ligand, which show comparable activity with cisplatin. Intracellular ROS accumulation in HeLa cells by DCFDA assay, together with the suppression of ROS accumulation and the rescue of cell viability by NAC, suggest that there may be a potential correlation between the increase in ROS generation and cytotoxicity of complex **3e**. Further cytotoxicity mechanism studies reveal that complex **3e** inhibits the proliferation of cancer cells in vitro via induction of apoptosis and G2/M phase cell cycle arrest. The absorption and fluorescence quenching spectroscopic studies, as well as viscosity measurements reveal that the interaction mode of complex **3e** with CT-DNA is minor groove binding and/or electrostatic interactions. The results of fluorescence titration and site marker competitive experiments on BSA suggest that complex **3e** can quench the fluorescence of BSA via a static quenching process and bind to BSA in Sudlow's site II. Above all, these results would be helpful in the design of new anticancer palladium(II) complexes.

Abbreviations

SAR	Structure–activity relationships
BSA	Bovine serum albumin
ROS	Reactive oxygen species
DMEM	Dulbecco's modified eagle's medium
FBS	Fetal bovine serum
MTT	3-(4,5-dimethylthiazol-2-yl)-2,5-diphenyl tetrazolium bromide
DCFH-DA	2′,7′-dichlorodihydrofluoroscein diacetate
CT-DNA	Calf-thymus DNA
FITC	Fluorescein isothiocyanate
PI	Propidium iodide
JC-1	5,5′,6,6′-tetrachloro-1,1′,3,3′-tetraethylbenzimidazolcarbocyanine iodide
TMS	Tetramethylsilane
HeLa	Human cervical epithelial carcinoma cell lines
MCF-7	Human breast adenocarcinoma cell lines
MGC803	Human gastric cancer cell lines
NAC	*N*-acetylcysteine
DMSO	Dimethyl sulfoxide
OD	Optical density
DCF	2′,7′-dichlorofluoroscein
PBS	Phosphate-buffered saline
CCCP	*m*-chlorophenylhydrazone
EB	Ethidium bromide
TrxR	Thioredoxin reductase
HSQC	Heteronuclear single-quantum correlation
HMBC	Heteronuclear multiple-bond correlation
MDR	Multidrug resistant
MPT	Mitochondrial permeability transition
HSA	Human serum albumin
DTNB	5,5′-dithiobis-2-nitrobenzoic acid

Acknowledgements

This work was supported by the Natural Science Foundation of Hebei Province (B2019201333, B2019201444) and the Key Basic Research Special Foundation of Science Technology Ministry of Hebei Province (15962602D).

References

[1] L. Kelland, Nat. Rev. Cancer 7 (2007) 573–584.
[2] Y.P. Ho, S.C. Au-Yeung, K.K.W. To, Med. Res. Rev. 23 (2003) 633–655.
[3] T.C. Johnstone, K. Suntharalingam, S.J. Lippard, Chem. Rev. 116 (2016) 3436–3486.
[4] J. Reedijk, Eur. J. Inorg. Chem. 10 (2009) 1303–1312.
[5] E.J. Gao, C. Liu, M.C. Zhu, H.K. Lin, Q. Wu, L. Liu, Anti Cancer Agents Med. Chem. 9 (2009) 356–368.
[6] L.L. Ma, W. Peng, J.J. Wang, X.Y. Yang, S.H. Li, S.X. Wang, J.C. Zhang, Sci. Sin. Chim. 44 (2014) 423–436.
[7] T. Lazarević, A. Rilak, Ž.D. Bugarčić, Eur. J. Med. Chem. 142 (2017) 8–31.
[8] M.N. Alam, F. Huq, Coord. Chem. Rev. 316 (2016) 36–67.
[9] M. Fanelli, M. Formica, V. Fusi, L. Giorgi, M. Micheloni, P. Paoli, Coord. Chem. Rev. 310 (2016) 41–79.
[10] K. Karami, M. Rafiee, Z.M. Lighvan, M. Zakariazadeh, A.Y. Faal, S.A. Esmaeili, A.A. Momtazi-Borojeni, J. Mol. Struct. 1154 (2018) 480–495.
[11] E.R. Reddy, R. Trivedi, A.V.S. Sarma, B. Sridhar, H.S. Anantaraju, D. Sriram, P. Yogeeswarid, N. Nagesh, Dalton Trans. 44 (2015) 17600–17616.
[12] D. Pucci, R. Bloise, A. Bellusci, S. Bernardini, M. Ghedini, S. Pirillo, A. Valentini, A. Crispini, J. Inorg. Biochem. 101 (2007) 1013–1022.
[13] Z.D. Bugarcic, J. Bogojeski, R. van Eldik, Coord. Chem. Rev. 292 (2015) 91–106.
[14] T.T.H. Fong, C.N. Lok, C.Y.S. Chung, Y.M.E. Fung, P.K. Chow, P.K. Wan, C.M. Che, Angew. Chem. Int. Ed. 55 (2016) 11935–11939.
[15] J. Kljun, I. Turel, Eur. J. Inorg. Chem. 2017 (2017) 1655–1666.
[16] A. Pasini, F. Zunino, Angew. Chem. Int. Ed. 26 (1987) 615–624.
[17] J.K. Barton, Science 233 (1986) 727–734.
[18] F. Trecourt, B. Gervais, O. Mongin, C. Le Gal, F. Mongin, G. Queguiner, J. Org. Chem. 63 (1998) 2892–2897.
[19] F. Mongin, F. Trecourt, B. Gervais, O. Mongin, G. Queguiner, J. Org. Chem. 67 (2002) 3272–3276.
[20] M. Stadler, F. Bauch, T. Henkel, A. Muhlbauer, H. Muller, F. Spaltmann, K. Weber, Arch. Pharm. 334 (2001) 143–147.
[21] J. Sheikh, A. Parvez, H. Juneja, V. Ingle, Z. Chohan, M. Youssoufi, T.B. Hadda, Eur. J. Med. Chem. 46 (2011) 1390–1399.
[22] H. Bischoff, M.R. Berger, B.K. Keppler, D. Schmahl, J. Cancer Res. Clin. Oncol. 113 (1987) 446–450.
[23] T. Schilling, K.B. Keppler, M.E. Heim, G. Niebch, H. Dietzfelbinger, J. Rastetter, A.R. Hanauske, Investig. New Drugs 13 (1995) 327–332.
[24] A. Muscella, N. Calabriso, F.P. Fanizzi, S.A. De Pascali, L. Urso, A. Ciccarese, D. Migoni, S. Marsigliante, Br. J. Pharmacol. 153 (2008) 34–49.
[25] A. Muscella, N. Calabriso, C. Vetrugno, L. Urso, F.P. Fanizzi, S.A. De Pascali, S. Marsigliante, Br. J. Pharmacol. 160 (2010) 1362–1377.
[26] A. Muscella, N. Calabriso, C. Vetrugno, F.P. Fanizzi, S.A. De Pascali, C. Storelli, S. Marsigliante, Biochem. Pharmacol. 81 (2011) 91–103.
[27] A. Muscella, N. Calabriso, C. Vetrugno, F.P. Fanizzi, S.A. De Pascali, S. Marsigliante, Biochem. Pharmacol. 81 (2011) 1271–1285.
[28] J.J. Wilson, S.J. Lippard, J. Med. Chem. 55 (2012) 5326–5336.
[29] J.D.C. Almeida, D.A. Paixao, I.M. Marzano, J. Ellena, M. Pivatto, N.P. Lopes, A.M.D.C. Ferreira, E.C. Pereira-Maia, S. Guilardi, W. Guerra, Polyhedron 89 (2015) 1–8.
[30] S.S. Bhat, A.A. Kumbhar, H. Heptullah, A.A. Khan, V.V. Gobre, S.P. Gejji, V.G. Puranik, Inorg. Chem. 50 (2011) 545–558.
[31] P.S. Lopes, D.A. Paixão, F.C.S. de Paula, A.M.D.C. Ferreira, J. Ellena, S. Guilardi, E.C. Pereira-Maia, W. Guerra, J. Mol. Struct. 1034 (2013) 84–88.
[32] B. Weber, A. Serafin, J. Michie, C.E.J. Van Rensburg, J.C. Swarts, L. Bohm, Anticancer Res. 24 (2004) 763–770.
[33] N. Falzone, L. Bohm, J.C. Swarts, C.E.J. Van Rensburg, Anticancer Res. 26 (2006) 147–152.
[34] A. Hussain, S. Gadadhar, T.K. Goswami, A.A. Karande, A.R. Chakravarty, Eur. J. Med. Chem. 50 (2012) 319–331.
[35] A. Hussain, S. Gadadhar, T.K. Goswami, A.A. Karande, A.R. Chakravarty, Dalton Trans. 41 (2012) 885–895.
[36] K.Z. Zhang, S.S. Cui, J.J. Wang, X.H. Wang, R. Li, Med. Chem. Res. 21 (2012) 1071–1076.
[37] A. Wu, D.C. Kennedy, B.O. Patrick, B.R. James, Inorg. Chem. Commun. 6 (2003) 996–1000.
[38] R. Fernández, M. Melchart, A. Habtemariam, S. Parsons, P.J. Sadler, Chem. Eur. J. 10 (2004) 5173–5179.
[39] M. Melchart, A. Habtemariam, S. Parsons, P.J. Sadler, J. Inorg. Biochem. 101 (2007) 1903–1912.
[40] C.A. Vock, A.K. Renfrew, R. Scopelliti, L. Juillerat-Jeanneret, P.J. Dyson, Eur. J. Inorg. Chem. 2008 (2008) 1661–1671.
[41] S. Seršen, J. Kljun, K. Kryeziu, R. Panchuk, B. Alte, W. Körner, P. Heffeter, W. Berger, I. Turel, J. Med. Chem. 58 (2015) 3984–3996.
[42] A. Valentini, F. Conforti, A. Crispini, A.D. Martino, R. Condello, C. Stellitano, G. Rotilio, M. Ghedini, G. Federici, S. Bernardini, D. Pucci, J. Med. Chem. 52 (2009) 484–491.
[43] Y.C. Li, Z.Y. Gu, C. Zhang, S.H. Li, L. Zhang, G.Q. Zhou, S.X. Wang, J.C. Zhang, Eur. J. Med. Chem. 144 (2018) 662–671.
[44] F. Caruso, R. Pettinari, M. Rossi, E. Monti, M.B. Gariboldi, F. Marchetti, C. Pettinari, A. Caruso, M.V. Ramani, G.V. Subbaraju, J. Inorg. Biochem. 162 (2016) 44–51.
[45] N. A.A. Ali, R. Jansen, H. Pilgrim, K. Liberra, U. Lindequist, Phytochemistry 41 (1996) 927–929.
[46] N.A.A. Ali, R.A.A. Mothana, A. Lesnau, H. Pilgrim, U. Lindequist, Fitoterapia 74

(2003) 483–485.
[47] G.J. Huang, J.S. Deng, C.S. Chiu, J.C. Liao, W.T. Hsieh, M.J. Sheu, C.H. Wu, J. Evid. Based Complement. Altern. Med. 2012 (2012) 480714.
[48] H.Y. Chang, M.J. Sheu, C.H. Yang, T.C. Lu, Y.S. Chang, W.H. Peng, S.S. Huang, G.J. Huang, J. Evid. Based Complement. Altern. Med. 2011 (2011) 478246.
[49] J. Ravindran, G.V. Subbaraju, M.V. Ramani, B. Sung, B.B. Aggarwal, Biochem. Pharmacol. 79 (2010) 1658–1666.
[50] W. Chen, Z. Zhao, L. Li, B. Wu, S.F. Chen, H. Zhou, Y. Wang, Y.Q. Li, Free Radic. Biol. Med. 45 (2008) 60–72.
[51] Q. Wu, Y. Kang, H. Zhang, H.M. Wang, Y.H. Liu, J. Wang, Biochem. Biophys. Res. Commun. 453 (2014) 385–391.
[52] Y.C. Chen, H.Y. Chang, J.S. Deng, J.J. Chen, S.S. Huang, I.H. Lin, W.L. Kuo, W. Chao, G.J. Huang, Am. J. Chin. Med. 41 (2013) 1439–1457.
[53] G.J. Huang, J.S. Deng, S.S. Huang, M.L. Hu, J. Agric. Food Chem. 59 (2011) 7104–7113.
[54] M.C. Hsin, Y.H. Hsieh, P.H. Wang, J.L. Ko, I.L. Hsin, S.F. Yang, Cell Death Dis. 8 (2017) 3089.
[55] P. Chethna, S.S. Iyer, V.V. Gandhi, A. Kunwar, B.G. Singh, A. Barik, N.V. Balaji, M.V. Ramani, G.V. Subbaraju, K.I. Priyadarsini, ACS Omega 3 (2018) 5958–5970.
[56] R. Pettinari, F. Marchetti, A. Petrini, C. Pettinari, G. Lupidi, P. Smolenski, R. Scopelliti, T. Riedel, P.J. Dyson, Organometallics 35 (2016) 3734–3742.
[57] R.S. Kumar, S. Arunachalam, V.S. Periasamy, C.P. Preethy, A. Riyasdeen, M.A. Akbarsha, J. Inorg. Biochem. 103 (2009) 117–127.
[58] N.V. Balaji, M.V. Ramani, A.G. Viana, L.P. Sanglard, J. White, V. Mulabagal, C. Lee, T.J. Gana, N.O. Egiebor, G.V. Subbaraju, A.K. Tiwari, Bioorg. Med. Chem. 23 (2015) 2148–2158.
[59] J.Y. Feng, Z.Q. Liu, Eur. J. Med. Chem. 46 (2011) 1198–1206.
[60] S. Wimmer, P. Castan, F.L. Wimmer, N.P. Johnson, J. Chem. Soc. Dalton Trans. (1989) 403–412.
[61] E. Bremer, G. van Dam, B. Jan Kroesen, L. de Leij, W. Helfrich, Trends Mol. Med. 12 (2006) 382–393.
[62] Q.B. Cui, J.Q. Wang, Y.G. Assaraf, L. Ren, P. Gupta, L.Y. Wei, C.R. Ashby Jr., D.H. Yang, Z.S. Chen, Drug Resist. Updat. 41 (2018) 1–25.
[63] H.Y. Huang, B.L. Yu, P.Y. Zhang, J.J. Huang, Y. Chen, G. Gasser, L.N. Ji, H. Chao, Angew. Chem. Int. Ed. 54 (2015) 14049–14052.
[64] J.D. Ly, D.R. Grubb, A. Lawen, Apoptosis 8 (2003) 115–128.
[65] G.I. Evan, K.H. Vousden, Nature 411 (2001) 342–348.
[66] L.M. Guachalla, K.L. Rudolph, Cell Cycle 9 (2010) 4058–4060.
[67] S.P. Jackson, J. Bartek, Nature 461 (2009) 1071–1078.
[68] D. Ćoćić, S. Jovanović, M. Nišavić, D. Baskić, D. Todorović, S. Popović, Ž.D. Bugarčić, B. Petrović, J. Inorg. Biochem. 175 (2017) 67–79.
[69] D. Ćoćić, S. Jovanović, S. Radisavljević, J. Korzekwa, A. Scheurer, R. Puchta, D. Baskić, D. Todorović, S. Popović, S. Matić, B. Petrović, J. Inorg. Biochem. 189 (2018) 91–102.
[70] J.G. Liu, Q.L. Zhang, X.F. Shi, L.N. Ji, Inorg. Chem. 40 (2001) 5045–5050.
[71] W.J. Mei, J. Liu, H. Chao, L.N. Ji, Transit. Met. Chem. 28 (2003) 852–857.
[72] B.C. Baguley, E.M. Falkenhaug, Nucleic Acids Res. 5 (1978) 161–171.
[73] D.L. Boger, B.E. Fink, S.R. Brunette, W.C. Tse, M.P. Hedrick, J. Am. Chem. Soc. 123 (2001) 5878–5891.
[74] R. Palchaudhuri, P.J. Hergenrother, Curr. Opin. Biotechnol. 18 (2007) 497–503.
[75] T. Sarwar, M.A. Husain, S.U. Rehman, H.M. Ishqi, M. Tabish, Mol. BioSyst. 11 (2015) 522–531.
[76] B.M. Zeglis, V.C. Pierre, J.K. Barton, Chem. Commun. (2007) 4565–4579.
[77] C.A. Franklin, J.V. Fry, J.G. Collins, Inorg. Chem. 35 (1996) 7541–7545.
[78] Y.P. Li, Y.B. Wu, J. Zhao, P. Yang, J. Inorg. Biochem. 101 (2007) 283–290.
[79] G. Fanali, A. di Masi, V. Trezza, M. Marino, M. Fasano, P. Ascenzi, Mol. Asp. Med. 33 (2012) 209–290.
[80] H.L. Hao, X.C. Liu, X.X. Ge, Y. Zhao, X. Tian, T. Ren, Y. Wang, C.F. Zhao, Z. Liu, J. Inorg. Biochem. 192 (2019) 52–61.
[81] D. Senthil Raja, N.S.P. Bhuvanesh, K. Natarajan, Dalton Trans. 41 (2012) 4365–4377.
[82] A. Shanmugapriya, Ruchi Jain, D. Sabarinathan, G. Kalaiarasi, F. Dallemer, R. Prabhakaran, New J. Chem. 41 (2017) 10324–10338.
[83] K. Karami, Z.M. Lighvan, S.A. Barzani, A.Y. Faal, M. Poshteh-Shirani, T. Khayamian, V. Eigner, M. Dušek, New J. Chem. 39 (2015) 8708–8719.
[84] F.F. Tian, F.L. Jiang, X.L. Han, C. Xiang, Y.S. Ge, J.H. Li, Y. Zhang, R. Li, X.L. Ding, Y. Liu, J. Phys. Chem. B 114 (2010) 14842–14853.
[85] G. Sudlow, D.J. Birkett, D.N. Wade, Mol. Pharmacol. 12 (1976) 1052–1061.
[86] F.F. Tian, J.H. Li, F.L. Jiang, X.L. Han, C. Xiang, Y.S. Ge, L.L. Li, Y. Liu, RSC Adv. 2 (2012) 501–513.
[87] K. Karami, Z.M. Lighvan, M.D. Jahromi, J. Lipkowski, A.A. Momtazi-borojeni, J. Organomet. Chem. 827 (2017) 1–14.
[88] K. Karami, M. Rahimi, M. Zakariazadeh, O. Buyukgungor, Z. Amirghofran, J. Organomet. Chem. 878 (2018) 60–76.
[89] A. Holmgren, J. Biol. Chem. 252 (1977) 4600–4606.
[90] G.L. Parrilha, K.S.O. Ferraz, J.A. Lessa, K.N. de Oliveira, B.L. Rodrigues, J.P. Ramos, E.M. Souza-Fagundes, I. Ott, H. Beraldo, Eur. J. Med. Chem. 84 (2014) 537–544.